Recent Trends in Fibrous Material Science

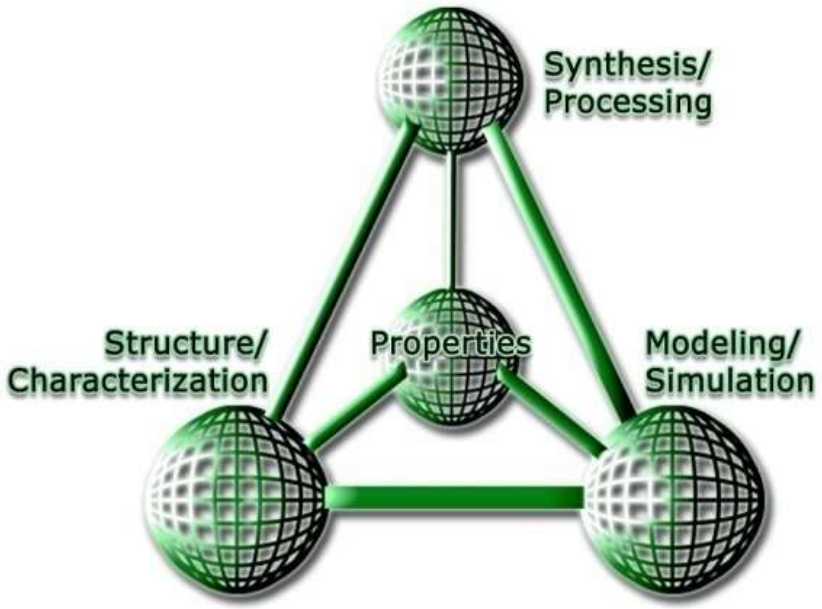

Volume - V
September - 2019

Key Authors and Editors

Rajesh Mishra
Jiri Militky

TECHNICKÁ UNIVERZITA V LIBERCI
Fakulta textilní

TECHNICAL UNIVERSITY OF LIBEREC
Faculty of Textile Engineering

TECHNICKÁ UNIVERZITA V LIBERCI
Textilní fakulta Katedra materiálového inženýrství

Doc. Rajesh Mishra, B.Tech., PhD
Prof. Ing. Jiří Militký, CSc. EURING

RECENT TRENDS IN FIBROUS MATERIAL SCIENCE

Liberec 2019

Chapter 4

Conductive Nanoparticles for the Automotive Industry

Mohanapriya Venkataraman, Jiří Militký, Divan Coetzee, Rajesh Mishra, Dana Křemenáková
Faculty of Textile Engineering, Dept. of Material Engineering, Studentská 2, Technical University of Liberec 461 17 Czech Republic

1. INTRODUCTION

Conductive nanoparticles are used in many forms for various purposes. These range from thermal conductivity for heat transfer or insulation purposes, electrical conductivity or a combination thereof as both aspects can have an influence on each other. Various articles have been reviewed as cited. During this review the characterization, manufacturing, properties, methods, results and applications are discussed. Silver nanoparticles (AgNPs) are used extensively for both thermal conductivity and electrical conductivity. It is one of the most commonly used nanomaterials in industry while the popularity of carbon nanomaterials is increasing drastically. Phase change materials rely more on the thermal conductivity of nanoparticles; however, this property can be influenced by electrical conductivity. Conductivity of composites can be related to the formation of conductive pathways as nanofiller materials make contact with each other. Discussed literature comes from various fields of applications, however properties exhibited by the findings may be applied in the automotive industry as certain characteristics such as phase changes, dimensional stability, magnetization and modulus changes of composites can be of benefit for other applications. With increasing use of nanomaterials and relatively little understanding of the environmental impact thereof, disposal and recyclability become of more importance as discussed.

1.1 Characterization, Manufacturing and Properties

Nanoparticles are inorganic or organic particles with dimensions below 100 µm with properties depending on their size which include optical, magnetic or electrical properties. This definition restricts true nanoparticles to particles with dimensions in the range of 10 nm-20 nm. The theory states that with a decrease in particle size the ratio of the surface area of the particle respective to its volume increases exponentially resulting in an influence of surface-, interfacial properties and agglomeration. Depending on the nanoparticle size introduced to the polymer matrix this can alter the electrical and thermal conductivity, polymer phase behavior and stability, mechanical properties, flame retardancy, density, magnetic, optic or dielectric properties of the polymer matrix. It was noted [1] that the refractive index of PbS nanoparticles with sizes below 25 nm was significantly less compared to larger particles. For SnO_2 a significant increase in energy band gap was observed with a

decrease in particle size. For ZrO_2 a decrease in particle size resulted in a decrease in transition temperatures which is typical for ceramics. A decrease in particle size for TiO_2 resulted in an increase in electrical storage capacity with similar effects observed for rutile particles. Size effects for dielectric properties were found in a different size range. A decrease in ferroelectric to para-electric phase transition in $PbZrO_3$ at particles sizes below 100 nm was observed as well as a decrease in dielectric constant. Below a particle size of 70 nm the para-electric phase was stable whilst above 100 nm the tetragonal ferroelectric phase was stable. This was as a result of pseudo-tetragonal distortion of the crystal lattice. Regarding the polymer-nanoparticle interface, when the two components experience attraction forces this will result in an increase of the glass transition temperature of the polymer matrix due to restricted mobility of the polymer chains. An increase in particle size at lower weight percentages up to 5% of Al_2O_3 and SiO_2 nanoparticles in a PEEK (polyetheretherketone) matrix resulted in an increase in tensile and compressive strength whilst flexural strength was unaffected. With a decrease in nanoparticle size the degree of filling in the overall polymer will decrease correspondingly. The article also mentions the application of microsphere composite nanoparticles in biological and magnetic resonance applications, also referred to as hybrid nanoparticles in some cases. These microsphere composite nanoparticles are typically ceramic nanoparticles inside a hydrophobic polymer matrix and then encapsulated with a hydrophilic organic shell such as chitosan as depicted in fig. 1 [1].

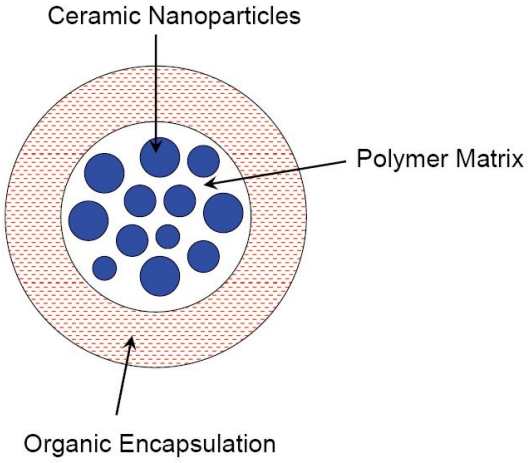

Fig. 1 Microsphere nanoparticle [1]

Composites combine the properties of a bulk material with that of a size dependent particle [2]. Composite formation techniques include ex situ, chemical in situ and physical in situ methods which leads to the final composite or the formation of hybrid nanoparticles. Ex situ processes are where nanoparticles are synthesized and introduced into the polymer matrix in solution. This process has a typical drawback of nanoparticle agglomeration which can be difficult to overcome and resolve, however this can be assisted using surfactants, which is a chemical dispersion method. Chemical in situ methods uses a liquid environment to generate the nanoparticles typically as hybrid particles or directly into the polymer matrix. This method typically

ensures a more homogeneous dispersion of the nanoparticles compared to the ex situ process. Physical in situ methods are mainly gas-phase methods used to produce encapsulated nanoparticles which appears as hybrid nanoparticles. This method applies energy which transforms a precursor gas of chemical compounds into inorganic nanoparticles. In subsequent coating step the organic compounds are grafted onto the formed nanoparticle surfaces for coating, encapsulation or surface functionalization [1].

Composites can be classified as either Ceramic Matrix Nanocomposites (CMNC), Metal Matrix Nanocomposites (MMNC) or Polymer Matrix Nanocomposites (PMNC) to which nanoparticles can be added to either enhance, change or add to the properties of the matrix material. Most of the properties associated with nanoparticles as discussed in this article can be attributed to particle size [3]. The effect of particle size on the various matrix properties are presented in table 1 below.

Table 1. Effect of nanoparticle size on various matrix properties [3]

Properties	Feature size (nm) at which changes might be expected
Catalytic activity	<5
Making hard magnetic materials soft	<20
Producing refractive index changes	<50
Producing super paramagnetism and others electromagnetic phenomena	<100
Producing strengthening and toughening	<100
Modifying hardness and plasticity	<100

1.2 Nanoparticle containing hydrogels

Another aspect for the use of nanoparticles is for use in hydrogels has been investigated [4]. Hydrogels exhibit properties such as swelling and shrinking over several orders of magnitude dependent on certain stimuli. These typically form a cross-linked polymer network which is highly sensitive to stimuli such as light, solvent composition, solutes, pH, temperature and electric fields. Significant changes in mechanical property and thermal response was observed in poly *N* -isopropyl amide hydrogels with the incorporation of gold nanoparticles dispersed in the hydrogel. Typical approaches for producing the nanoparticle imbedded in the hydrogel is to use preformed nanoparticles and adding it to a hydrogel monomer forming solution. The composition can vary depending on the desired properties. It is important to keep the crosslink density of the polymer matrix high in order to prevent nanoparticle leaching. This process results in three different types of nanoparticle imbedded hydrogels as illustrated in fig. 2 below. Fig. 2 (a) represents the nanoparticle or microparticle stabilizing an inorganic polymer matrix or other

polymer nanoparticles. (b) nanoparticles non-covalently dispersed in a hydrogel matrix and (c) nanoparticles which are covalently dispersed in a hydrogel matrix [4].

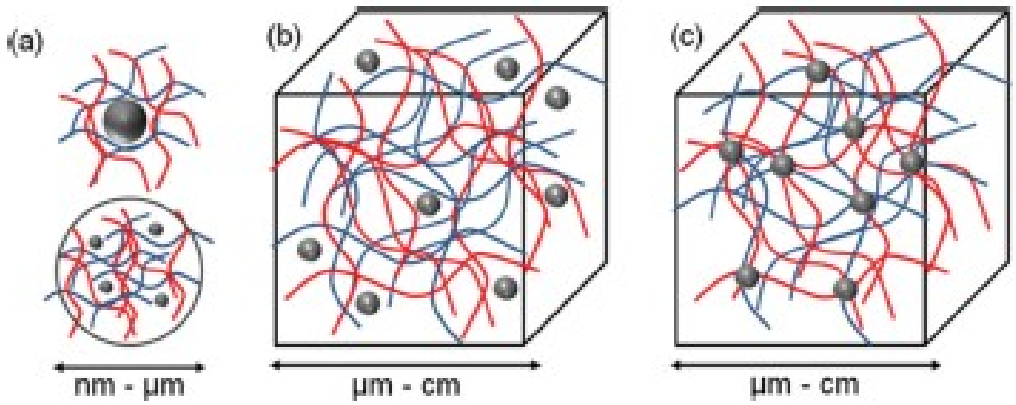

Fig. 2 Different nanoparticle/hydrogel materials [4]

Different approaches to obtaining these are illustrated in fig. 3 below as briefly discussed previously. In fig. 3 five different methods are depicted including the most common already mentioned.

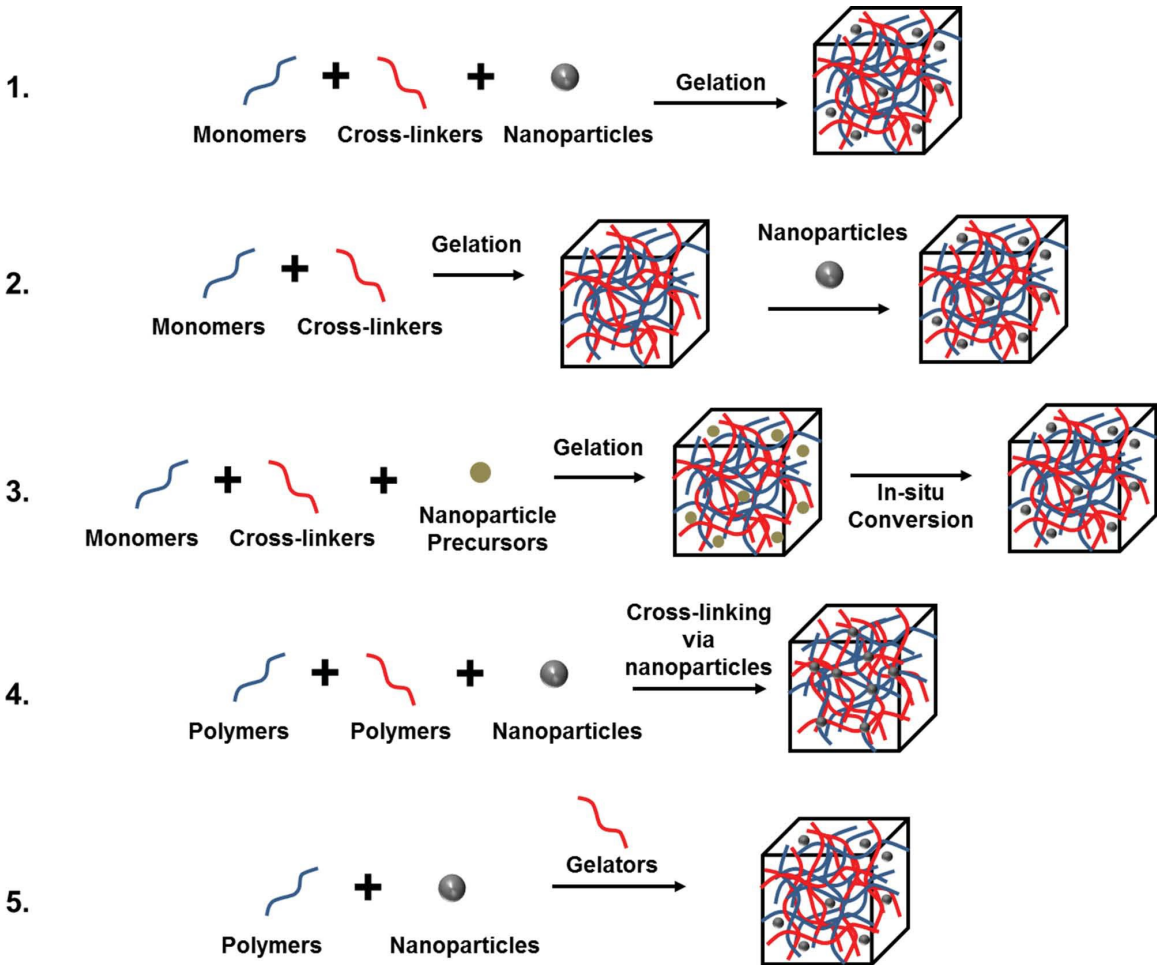

Fig. 3 Different methods of obtaining nanoparticle hydrogel materials [4]

Typical nanoparticle incorporation as depicted in fig. 3 above use nanomaterials such as silver nanoparticles which operates in the same mechanisms and properties as discussed in the silver nanoparticle section of this article with antimicrobial, pH

sensitive and conductive properties. Gold nanoparticles greatly influence the thermal conductivity of the material whilst also imposing antibacterial properties. This has proven to influence the swelling and shrinking of the hydrogel significantly, however it is noted that care must be taken on the hydrogel used since typical drawbacks are experienced such as when an applied temperature may cause a phase change of the hydrogel. The cost of using gold in certain applications makes it unfeasible. Using cobalt and copper nanoparticles could produce a hydrogel which is magnetically sensitive whilst also proving to poses antibacterial properties. A metal oxide nanoparticle also presents magnetic and conductive properties and are used in medicinal applications to mimic muscle movements. The use of non-metal nanoparticle hydrogels has been associated with catalysis of functional materials such as in the case of using carbon-based nanoparticles to improve drug release whilst providing similar function as metal-based nanoparticles at a lower cost. The combination of using polymer nanoparticles with a polymeric component different to that of the hydrogel has proven to incorporate properties of the added polymer. This resulted in improvement of desired properties such as mechanical strength and other physical properties of the hydrogel depending on the properties of the polymeric nanoparticle additive [4]. All the mentioned applications are based on previous research with specific applications, however the properties of the material expanding and contracting, conducting and magnetizing under different stimuli can be used in many other industrial applications.

1.3 Thermally conductive nanoparticles for phase change materials

Phase change materials (PCMs) have been used extensively due to their capacity to store and release large amounts of thermal energy by promoting a phase change from a solid to melted phase at a specific temperature. This is due to the materials thermal conductivity (TC) which influences the melting-solidification rate also referred to as the charging and discharging rate. The addition of nanoparticles could increase or decrease the thermal conductivity of a material or liquid, as according to Salaün et al. [5], since it is also dependent on the matrix in which the nanoparticles are placed resulting in a raising or reduction temperature effect on the melting-solidification rate of the overall material [6]. Nano structured materials have been receiving more attention in recent years due to their advantageous properties which include lighter weight, no contact heat transfer problems, their availability of natural convection to enhance heat transfer during melting and recyclability of materials used. Nanostructured materials for this purpose are typically used in the form of nanoparticles, nanowires, nanotubes, nanofibers, etc. [7].

Silver nanoparticles (AgNP) proved to be a promising additive because of its ability to enhance thermal conductivity of organic phase change materials. Qian et al. [8] experimented with this property to be used in solar energy applications using PCMs since it was found to be the most effective method of latent heat storage. This is due to a higher density of heat that can be stored with a smaller temperature difference between storing and releasing heat energy. Organic PCMs are widely used due to higher latent heat density, suitable phase transition temperature, smaller temperature

swings, and reasonable cost also stable physical and chemical properties over long periods of use. Polyethylene glycol was one of the most studied PCMs, however several problems are associated with handling of the material during phase changes. This can be compensated for by packaging technology to produce a shape stabilized PCM. Another approach is encapsulation using inorganic materials for isolation; however, this is associated with high synthesis cost and physical aspects such as chemical stability and flammability. Shape stabilized PCMs adopt good thermal-conductive supporting materials with the ability to maintain a solid shape even when the temperature exceeds the melting temperature of the material. The authors observed that ss-PCMs prepared with diatomite has the greatest energy storing density, thermal conductivity, geological deposits, excellent absorption capacity, low density, chemical inertness, porous structure of 80 % - 90 % and low cost compared to other PCMs used in the building industry. One disadvantage is impurities blocking the pores of the raw materials, but significant improvement was made by treatment of the raw material using the facile alkali-leaching method. The TC was improved by the incorporation of the silver nanoparticles due to its high conductivity of 429 W m^{-1} K^{-1} [8].

Thermal interference composites contain both non electrically conductive micron sized fillers and electrically conductive nanoparticles which are blended with a polymer matrix as illustrated in figure 4. These fillers typically increases the bulk thermal conductivity of the polymer composite materials whilst decreasing the thermal interfacial resistances between the matrix material and the nanoparticle surface it is adhered to. Materials of this composition exhibit no electrical conductivity whilst the incorporation of nanoparticles promotes less phase separation of micron sized filler particles. This provides an electrically insulation material whilst facilitating heat transfer from the source. It is important that when applying the material to the heat source that no air gaps exists at the interface as this will inhibit the electrically insulation material from effectively removing the heat from the source. The invention states an organic polymer matrix comprised of either polydimethylsiloxane resins with any functional chemical elements, epoxy resins, acrylate resins, polyimide resins, fluorocarbon resins, benzocyclobutane resins fluorocarbon resins, fluorinated polyallelic ethers, polyamide resins, polyimidoamide resins, phenol resol resins, aromatic polyester resins, polypropylene ether resins, bismaleimide triazine resins, fluororesins and any other resins which are non-electrically conductive. These can be used in curable, gel, grease or phase change material form which can hold components together. The micron sized fillers are typically thermally conductive materials which can be reinforcing the polymer matrix or not and typically makes up between 10 % to 95 % of the final weight of the end material. These range in size from 1 – 100 microns although between 10 and 50 microns are preferred. These include fillers such as amorphous-, fumed or fused silica, quartz powder, carbon black, graphite, diamond, aluminum hydrates, metal nitrides, metal oxides or any combinations of the before mentioned. Electrically conductive nanoparticles are typically made from gold, aluminum, platinum, palladium, graphite, silver or copper. Semi conductive materials such as doped silicon

or silicon carbide can also be used. These range in size between 1 to 250 nanometres, however between 10 and 100 nm are preferred. To facilitate nanoparticle and filler binding to the organic polymer matrix a suitable solvent such as isopropanol, 1-methoxy-2-propanol, 1-methoxy-2-propyl acetate, toluene, xylene, n-methyl pyrrolidone, dichlorobenzene or any combination can be used. This is typically performed at temperatures ranging between 20 ºC and 140 ºC and under vacuum of 0.5 Torr – 250 Torr to remove any volatiles and excess solvent. This can be combined with a curing catalyst of about 10 ppm in the composition and less than 2% of the weight of the total curable composition. Examples of these catalysts include bisaryliodonium salts, radial curing catalysts or group 8-10 transition metals in the case of silicone resins. These may differ depending on the type of resin used. Nanoparticle containing (thermal interface materials) TIMs can have a thermal conductivity of up to 3 times that of TIMs which do not contain any nanoparticles. This is due to the creation of thermal conductive pathways between the micron sized filler particles which is enhanced by smaller pathways created by the conductive nanoparticles which typically comprises between 3-50 % of the overall polymer weight (fig. 4). Loading the polymer matrix with semi conductive nanoparticles in excess of 50 % weight might lead to a TIM which is able to conduct electricity effectively. High nanoparticle loads increase the viscosity of the polymer solution making it difficult to handle. Curing occurs by UV light, microwave or electron beam or combinations thereof at temperatures ranging between 20 ºC-250 ºC and under pressure of 1 atmosphere up to 5 tons per square inch, however typically this only goes up to 100 pounds per square inch for practical reasons. This occurs typically between 90 seconds and 60 minutes [9].

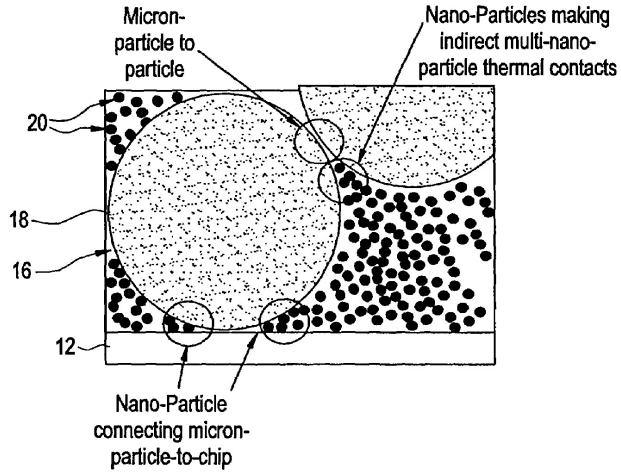

Fig. 4 Cross section of a composite containing nanoparticles [9]

1.4 Silver Nanoparticles

Silver nanoparticles also have an important function in medicine with extensive research performed on the antimicrobial properties thereof. Further investigation [10] also confirmed that the use of silver nanoparticles also exhibited anti-inflammatory properties. Xue et al. [11] experimented with the antimicrobial effects by

incorporation of silver nanoparticles onto cotton fibers while further modification of the silver nanoparticles added hydrophobicity to the finished textile to which the nanoparticles was applied. The mechanism of action regarding silver nanoparticles is not exactly known however various sources confirm viable theories. The suggested mechanisms include the anchoring of the silver nanoparticle onto the bacterial cell wall and subsequently penetrating it which changes the structure of the bacterial cell and eventually relates to cell death with further anchoring of silver nanoparticles. Silver nanoparticles also have the ability to produce free radicals which penetrates the bacterial cell walls making it more porous and causing cell death. Silver ions released by the nanoparticle could bind to thiol groups in the bacterial cell enzymes which are vital for the cell's growth. The binding of the silver ions to the thiol groups inhibits this growth ability of the bacterial cell and causes damage to the cell. It is not stated whether this action relates directly to cell death, but it does reduce the ability of the bacterial cell to repair itself. The silver ions also cause the generation of active oxygen species in the bacterial cell due to the inhibition of a respiratory enzyme. Silver is a soft acid and the reason for interacting so well by the previously stated mechanism is that the sulphur and phosphorous groups in the bacterial enzymes are soft bases which forms a chemically favorable reaction. These sulphur and phosphorous ions form the backbone of the bacterial DNA which is destroyed or altered by the binding of the silver ions. An area that requires more research is the potential effect of silver nanoparticles causing a reduction of the signal transduction in bacteria by the same binding mechanism to phosphorous containing proteins in the bacterial cell [10].

1.5 Electrically Conductive Nanoparticles

Conductive electrodes and electric circuits that remain stable under repetitive mechanical forces are highly desirable and typically used in the new era of flexible display technology, energy related devices, smart clothing and field effect transistors. Flexibility, electrical conductivity and strength are mutually exclusive parameters in designing a material. Mostly insulation techniques are used where the conductive material is covered with a flexible elastomer such as in the case of electric wiring. however, techniques are being developed to incorporate the conductive material inside the reinforcing structure to allow the material as a whole to conduct an electrical current. Park et al. [12] investigated the use of an SBS rubber fiber material impregnated with silver nanoparticles which was able to maintain effective bulk conductivity whilst overcoming large deformations. Applications of these include stretchable antennas or wearable electronics [12].

The conversion of thermal energy into electrical energy is known as thermoelectric conversion. This can result in the generation of electricity or electronic refrigeration. When a temperature gradient is applied to a thermoelectric couple consisting of elements which allows for the transportation of electrons (n-type) and is hole-transporting (p-type). Electrons diffuse from the warm end of the thermoelectric couple and will collect at the colder end which produces an electrostatic potential. The

ability of a material to perform this is called the Seebeck effect as illustrated in fig. 5(a) [13].

The opposite occurs when a voltage is applied to the thermocouple the electrons will attempt to arrange themselves as before the current was applied resulting in an absorption of energy at the applied side and releasing the energy at the other end as illustrated in figure 5 (b) above. This is also known as the Peltier effect. Advantages of this method are the absence of any moving parts as traditionally expected with electricity generation or refrigeration. Efficiency of thermoelectric materials are strongly associated with the ZT-value of the material where $ZT = (\alpha\ 2\ \sigma/\kappa)T$ which correlates to the electrical resistivity, thermal conductivity and absolute temperature as expressed in the equation in the same order of symbols. For high performance thermoelectric materials, the efficiency is also dependent on the materials ability to have a high electrical conductivity, a large Seebeck coefficient and low thermal conductivity which would result in a larger temperature difference between the ends at which stress is applied and released. This stress would relate to the application of a temperature difference or electrical current. By enhancing the ZT-value of a composite the system can rely less on thermal and electrical transport mechanisms which is the basis for a nanostructural approach to enhancing the thermoelectric performance of a material. Single crystals of nanoparticles exhibit the best electrical conductivity due to their absence of grain boundaries scattering charge carriers, however ZT-value optimization can only be achieved by elemental doping in order to adjust the carrier concentration.

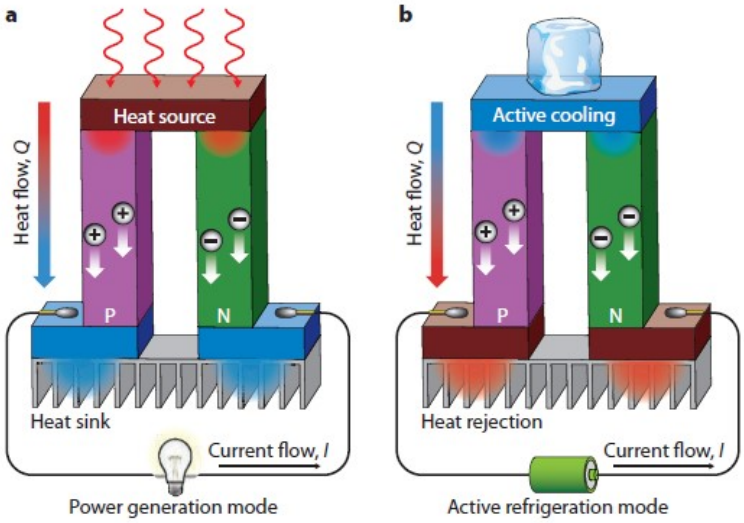

Fig. 5 Power generation and refrigeration cycles explaining the Seebeck and Peltier effects respectively [13]

When the size of the thermoelectric material is reduced especially to the nanoscale the system approaches a scale which can be compared to that of electron behavior in any direction. This increases the Seebeck coefficient of the material whilst reducing the thermal conductivity due to increased phonon scattering. For this reason, thermoelectrical materials on nanoscale typically shows thermal conductivity values

much lower than that of the bulk material as in the cases reported for Bi_2Te_3 and silicon nanowire between 10 nm - 20 nm. Thermal conductivity can also be reduced by the introduction of grain boundaries however; this will also decrease the carrier mobility reducing the efficacy of the material. Fig. 6 depicts the high thermoelectric performance of various materials at different temperatures mainly as a result of nanostructure engineering [13].

For an adequate amount of electrically conductive nanoparticles in a matrix to make it conductive the volume fraction of nanoparticles present must surpass that of the percolation threshold as illustrated in fig. 7 below for a silicon polymer matrix with electrically conductive nanoparticles. It is noted that with an increase in conductive nanoparticle volume fraction the electrical resistivity of the composite reduces significantly [14].

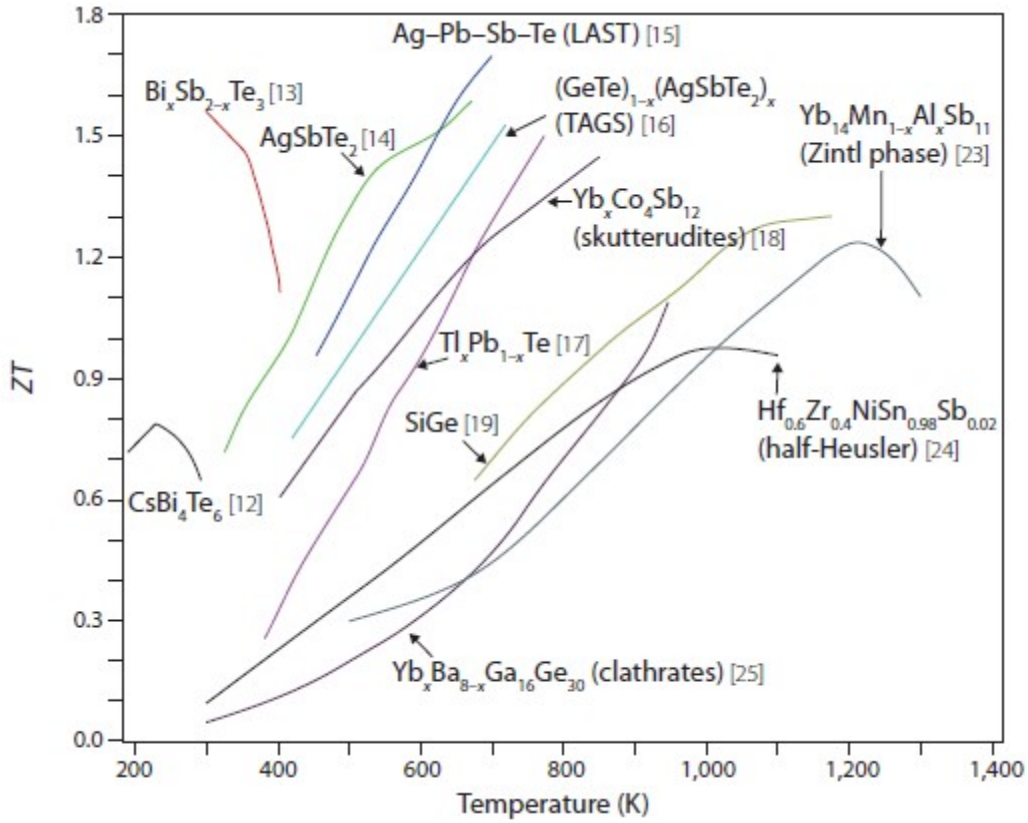

Fig. 6 Thermoelectric performance of various materials at different temperatures [13]

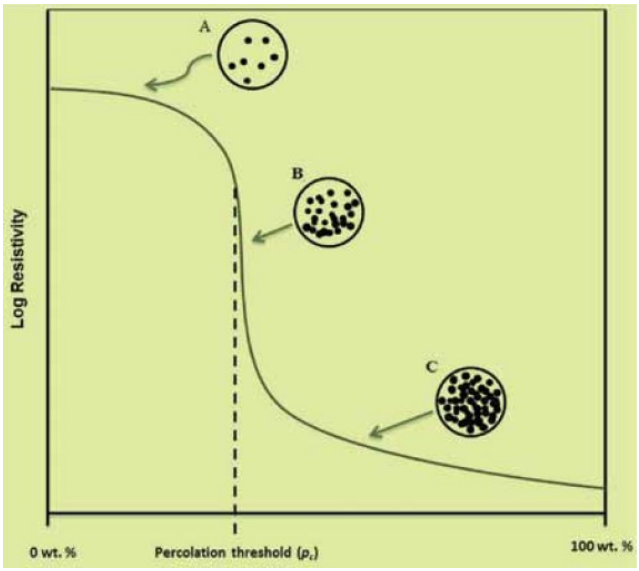

Fig. 7 Volume fraction of conductive nanoparticles effect on electrical resistivity [14]

It is not only the concentration as expressed in volume fraction of the nanoparticles that are important, but also their dispersion within the polymer matrix. Inadequate dispersion could lead to greater electrical resistance as well as mechanical failure. Nanoparticles dispersion can be classified under two main categories such as physical or chemical dispersion. Physical dispersion techniques include ultrasonic agitation which uses ultrasonic waves to vibrate the particles in order to move them away from each other. This causes nanoparticle dispersion in the matrix whilst allowing agglomerated particles to split which is a typical problem when using electrically conductive particles or particles with magnetic properties as they have a high attraction tendency. This method produces heat due to the vibration of particles and it therefore recommended to be performed in a thermal bath. This technique has been proven not to be suitable for dispersion of carbon nanotubes as they experience damage from the vibrations. Sheer mixing is preferred for viscous polymer matrices; however, this is typically performed using a magnetic stirrer and is therefore impractical for magnetically active metallic nanoparticles. Ball milling involves iron or plastic balls moving around in a rotary cylinder to break clusters of particles. This method is preferred for dispersion of carbon nanotubes for their high clustering rate, however improvements in this technique have been made to use micro sized balls to disperse nanoparticle agglomerates since it has a less damaging effect. This has been renamed to bead milling. Chemical dispersion methods include covalent and non-covalent techniques. Covalent techniques involve functionalization of the nanoparticles with hydroxyl and carboxyl functional groups which mainly works with a repulsion mechanism, however further research is investigating this method. Non-covalent methods are most commonly used with the use of surfactants to avoid nanoparticle aggregation [14].

Typically, SiO_2 nanoparticles exhibit poor electrical conductivity and microwave absorptive properties, however when heterogeneous nitrogen, carbon and chlorine atoms are incorporated on the surface these nanoparticles prove to be effective electrical conductors with the ability to absorb microwaves as a result of dielectric

loss due to the good electrical conductivity. This makes the particles suitable for applications such as wireless communications and anti-radar materials even when incorporated into a suitable noninterfering matrix [15].

Electromagnetic interference materials (EMI) are used in applications where electromagnetic radiation must be dissipated in order to prevent it from passing a specific boundary. This is done either via reflective or absorptive mechanisms depending on the materials used. Electromagnetic radiation increases with an increase in frequency. With increasing electromagnetic frequency, the ability for a metal to reflect decreases, whereas absorption increases. Metals such as copper, gold, silver and aluminum are excellent for reflective mechanisms whereas super molecular alloys and metals are effective electromagnetic radiation absorbers. These materials can be incorporated into a polymer matrix in the form of nanomaterials, with effectiveness increasing with higher volume fractions. It was also noted that spherical structures posed lower effectiveness and use of the filler material in flat/flake form yielded higher effectiveness at lower volume [16].

Silver nanoparticles are widely known for their excellent thermal and electrical conductivity. Dermanaki Farahani et al. [17] focused on the electrical conductivity of these nanoparticles for incorporation into a polymer matrix and used two coating methods onto a carbon fibre substrate to make it electrically conductive whilst also investigating the efficiency of the application technique. These were application by spraying the nanoparticle polymer solution or by casting. This applied nanoparticle polymer was used as a binder to which a second polymer was applied to fabricate a ternary biphasic nanocomposite for further improvement of mechanical resistance properties. These were performed with use of an annealing process. The produced materials pose potential aerospace applications such as shielding from electromagnetic interference and lighting strike protection [17].

1.6 Fiber Reinforced Composites with Conductive Nanoparticles

Fiber reinforced polymers are of increasing importance in industry due to their low weight and high strength properties. Typical applications include aircraft wings, turbine and rotor blades. These are typically designed to survive high stress levels for a lifespan of approximately 30 years or more. Failure detection in these systems can be very time consuming and costly whilst posing a potentially life-threatening danger if failure does occur. Studies by Böger et al., [18] incorporated electrically conductive carbon nanoparticles into a non-conductive epoxy matrix in order to detect possible failures in the non-conductive matrix electronically. This could also be applied to other nonconductive matrices [18]. The application potential of this property incorporated into the end use material could be incredibly useful in industry as it omits costly routine inspections and could produce an immediate warning with the use of an indicator in case of component failure.

Reasons for using nanomaterials instead of the conventional micro fillers for this type of application was investigated by Njuguna et al. [19]. It is stated that the micro fillers did provide significant improvement of mechanical properties to a reinforced material, but this was typically done at a sacrifice to the materials ductility.

Nanoparticles could improve even further on the enhancement of mechanical properties due to higher particle surface binding if used in the same volume rations compared to micro fillers whilst ductility is maintained in close relation to that of the unreinforced material. Advantages for both types of fillers depends on the desired property as it was found that incorporating nanoparticles increased the hardness and compression strength of the reinforced material, whilst reducing the materials rebound resilience. In comparison the addition of micro fillers was found to reduce the hardness and compression strength, while increasing the rebound resilience of the reinforced material.

As previously stated, the properties experienced using nanoparticles are mainly due to the effect of their small size, however their effect as a whole is dependent on the distance from one particle to another in the polymer matrix. It is stated that the closer the particles are together in a matrix the more improved is their contribution to the reinforcement of the composite as illustrated in fig. 8 [19].

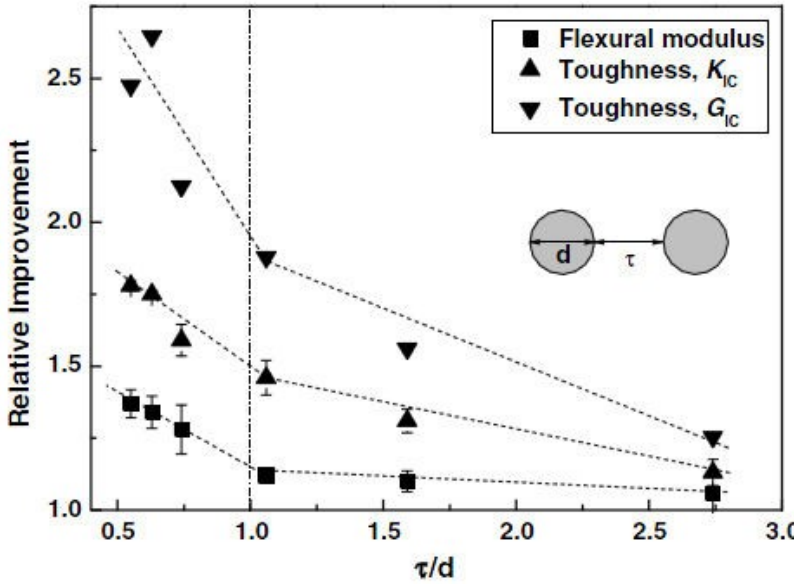

Fig. 8 Contribution of particle distance (t) over size (d) towards improvement of reinforcing matrix properties [19]

Particle stiffness also plays a role where more elastic nanoparticles improves the impact resistance of the reinforced matrix, however the modulus was decreased. The opposite was observed using stiffer nanoparticles [19].

1.7 Application of Nanoparticles in the Automotive Industry

Nanocomposite materials provide the possibility for great enhancements over current materials such as improving mechanical and electrical properties with a wide range of possible applications as illustrated in fig. 9.

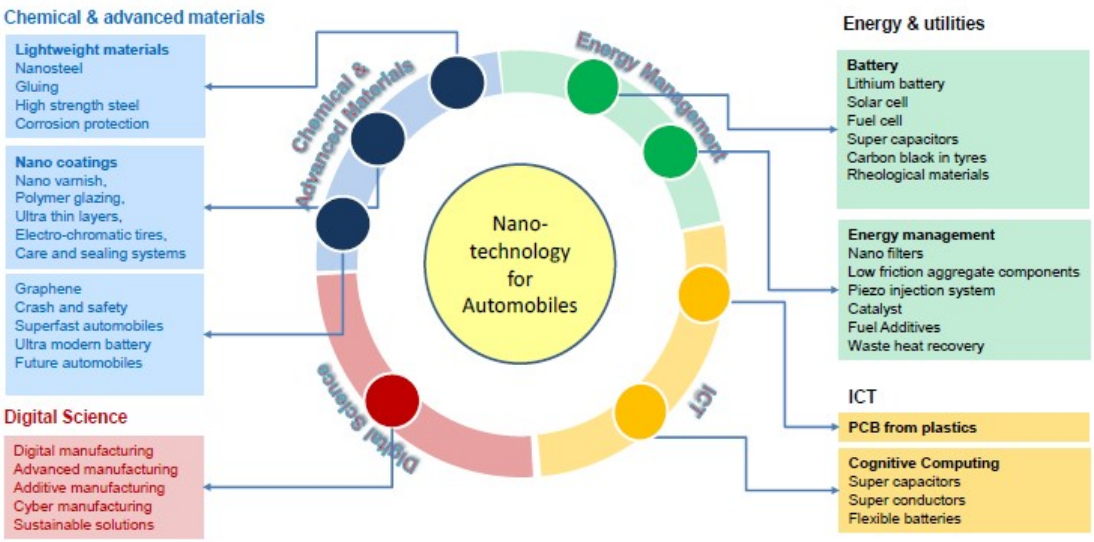

Fig. 9 Possible applications of nanocomposite materials in the automotive industry [20]

The use of nanocomposite plastic parts compared to highly filled plastic parts offer up to a 25% weight savings on average and as much as 80% over steel.

Approximately 90% of the total energy used by an automobile during its life cycle is from fuel consumed. The weight reduction offers significant advantages in cost saving to the consumer and in most cases to the manufacturer in terms of production efficiency and recyclability.

Enhanced properties include higher modulus, dimensional stability, heat distortion temperature, toughness and rheological properties as well as improved scratch ad mar resistance as illustrated for some composite materials in fig. 10 [21].

Resin type	Neat resin strength (MPa)	Neat resin modulus (GPa)	Nano-composite strength (MPa)	Nano-composite modulus (GPa)	Remarks
Epoxy (thermoset)	102-110	3.0-3.4	120-140	3.5-4.2	Flexural properties of solvent-based functionalized graphene (0.1 wt.%) nanocomposite.[18]
	53-58	2.7-3.0	75-80	3.6-3.9	Tensile properties of solvent-based graphene (0.1 wt%) nanocomposite[19]
Polyetherimide (amorphous thermoplastic)	79	2.6	126	4.7	*In situ* polymerization in 1.2 vol% single-walled carbon nanotube suspension in solvent. Although the matrix is amorphous, nanocomposites exhibit semi-crystallinity.[20]
Polyether ether ketone (PEEK)	88-90	2.0-2.2	85-90	3.3-3.4	Tensile properties of melt-extruded and injection-molded components after melt mixing with 7.5 wt % hydroxyapatite. [21]
Polypropylene (PP)	36-42	1.1-1.3	50-52	3.1-3.4	Flexural strength of solvent (isopropanol) based premixing of 10 vol % graphene platelets with powder PP followed by melt-mixing and extrusion. [22]
Nylon	69	1.1	107	2.1	Nylon 6/clay hybrid obtained by melt-mixing at 4.2 wt.% clay loading.[23]
Polycarbonate (PC)	120	2.0	160	2.7	Rolled fibers of multi-layered (320 aligned layers) graphene/PC (0.08 vol.%) nanocomposite film.[24]
Polymethyl methacrylate (PMMA)	70	2.1	77-86	3.6-4.0	Methanol-coagulated films from THF solution containing 1 wt.% functionalized (partially oxygenated) graphene sheets.[25]

Fig. 10 Modulus and strength improvements for various common composites [22]

Nanoclays are one of the most common nanoparticle additives with up to 80% used for composite formation in the automotive industry [23]. Carbon fiber, carbon nanotubes and polyhedral oligomeric silsesquioxanes are also common materials used in nanocomposite formation with increasing popularity, especially in the case of multiwall carbon nanotubes, as manufacturing costs decreases with new developments. The popularity for the use of nanoclays are driven by the need for low cost production since the price of nanoclays range from $6 to $8/kg compared to other nanomaterials. Nanoclay reinforced composites exhibit improved mechanical properties such as a good balance of stiffness and toughness. These materials also exhibit enhanced heat deflection temperatures without loss in elongation while color ability, scratch and mar resistance are improved. The use of nanoclays offers a reduction in weight and relative heat release, excellent flame retardancy with excellent dispersion and exfoliation. Commonly used polymer matrices are polyolefins, thermoplastics such as polyamide, polyphenylene sulphide, polyetheretherketone (PEEK), polyethylene terephthalate, polycarbonate, epoxy thermosets and block polymers such as styrene-butadiene. The use of thermoplastics as matrices are beneficial to the automotive industry due to its low cost, long shelf life, low weight, high performance properties which can be easily modified and recyclability. Thermoplastics offer enhanced fracture toughness over thermosets as well as enhanced mechanical, thermal, electrical and barrier properties. These materials can also be easily repaired by mechanical welding [23].

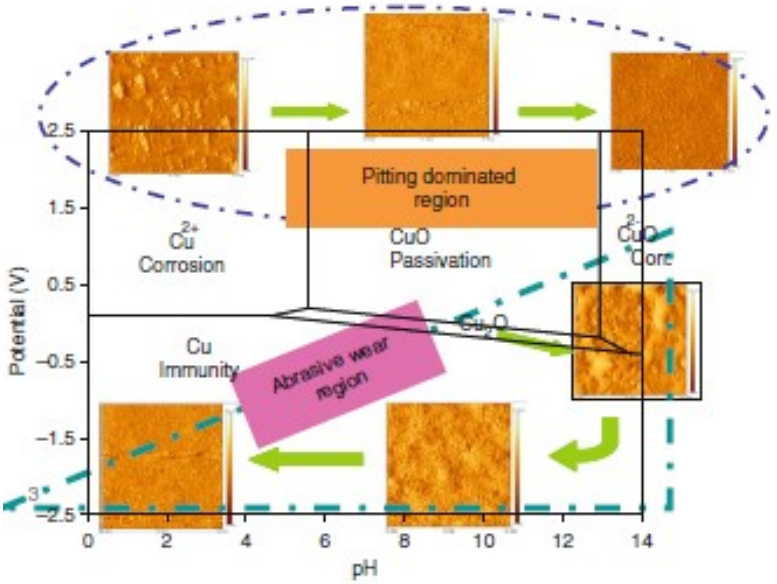

Fig. 11 Wear of copper as a result of mechanical polishing with changes in pH with polishing slurry [24]

Due to the thermal and electrically conductive properties of nanoparticles as discussed in this section the use of nanoparticles in applications such as motor oils, lubricants and polishes could be highly beneficial to the industry in terms of modification. Nanoparticles could exhibit abrasive characteristics depending on the type and size

used such as in the case of polishing slurries which are comprised of nanoparticles, oxidizer friction modifiers and other additives such as colorants or fragrances dissolved in deionized water. Combined these forms an effective tool in dirt removal from automotive components with the degree varying on differences in compositions mentioned. Fig. 11 depicts the wear cycle for copper as an effect of mechanical polishing with polishing slurry and how the chemical nature changes as a result of pH influence [24].

The service life of automotive components often depends on their surface properties. Improved surface properties allowed for the retaining of bulk characteristics which are necessary for such components to guarantee enhanced mechanical and tribological properties. In an article by Tonelli et al. [25] friction stir processing (FSP) was used to produce surface composites characterized by an extruded $AlSi_{12}CuNiMg$ matrix with micro and nano-sized Al_2O_3 particles for reinforcement. Multiple passes of FSP using two different strategies were applied to distribute the Al_2O_3 particles [25].

Friction Stir Processing (FSP) is a relatively new technique of applying a reinforcement matrix onto substrates as investigated by Mishra et al. [26] which is what an experiment by Tonelli et al. [25] was based on. According to the authors FSP was attempted to incorporate ceramic particles into a surface layer of aluminum alloy to form a surface composite. FSP has been developed for microstructural modification based on the basic principles of friction stir welding (FSW). FSW is a solid-state joining process developed initially for aluminum alloys.

The concept of FSP is rather uncomplicated since it involves a rotating tool with pin and shoulder which is inserted into a single piece of material for microstructural modification and this is traversed along the desired area or line to cover the region of where the composite is to be applied as illustrated in fig. 12 [26].

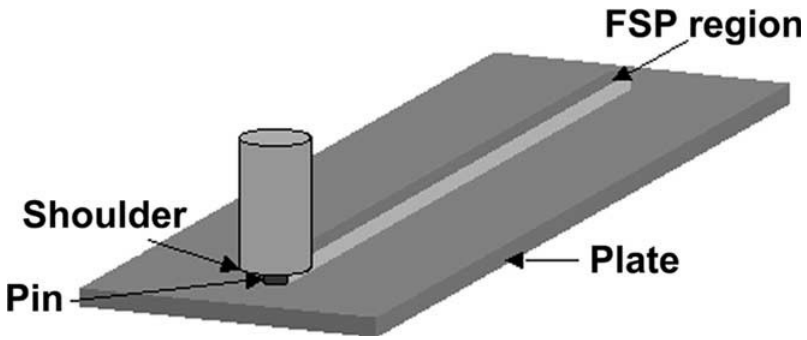

Fig. 12 Friction Stir Processing method of operation [26]

Localized heating occurs at the point of friction contact which softens and plasticizes the materials. By the movement of the pin a volume of processed material is produced by the materials grinding from the front to the back of the pin. This causes the applied material to undergo intense plastic deformation and results in significant grain refinement. Potential applications of FSP includes to generate a microstructure which is amenable to a high strain rate super plasticity [26].

Diesel engines are typically associated with durability, reliability and fuel economy; however, they tend to produce hazardous emissions of particle matter and nitric

oxides. Something that engine manufacturers have been struggling with for decades and becoming more problematic due to higher environmental restrictions imposed. Various methods of reducing these hazardous emissions can be used such as incorporating nanoparticles into the fuel mixture or in use of an exhaust filter system. An article by Roy et al. [27] examined the use of multiwalled carbon nanotubes (MWCNT) to reduce the emissions associated with these gasses.

Along with the ability to reduce emissions applications regarding the service life of automotive components the use of carbon nanotubes have been used as filler material in plastic materials for reinforcement, fire protection and heat insulation which could also be applied in the industry.

1.8 Environmental Impact

With more composite materials used today and annual production increasing waste of these materials are becoming of more concern. Especially in the case of carbon fiber which has a high modulus and resistance to degradation making disposal and reutilization difficult. Even as waste carbon fiber still has adequate mechanical properties to be used in further applications. These can be used as reinforcement in materials with lower mechanical requirements as the parent application or simply by removing defects. Commonly the waste material can be mechanically degraded to form a powder to be used as filler with further processing leading to carbon-based nanoparticles. These can be used in any of the previously mentioned applications where similar material was used whilst the nanoparticles can also act as reinforcement to other recycled materials such as recycled polymers which typically loses mechanical strength upon recycling due to polymer chain breakage [28]. Some preliminary studies have been conducted on how drilling affects the release of nanoparticles since our understanding of the toxicology thereof is still limited [29].

2 EXPERIMENTAL METHODS, RESULTS AND DISCUSSION

2.1 Thermally Conductive Nanoparticles for Phase Change Materials

Motahar et al. [7] used mesoporous silica ($MPSiO_2$) due to its fascinating porous and morphological characteristics to investigate the thermal conductivity of the PCM. The $MPSiO_2$ was dispersed in n-octadecane and the rheological behavior was examined. N-octadecane required degassing due to its high dissolved air content followed by the addition of nanoparticles and melting under vacuum. The PCM was stirred using a mechanical stirrer at 1000 rpm and 50 ^oC followed by sonication to ensure uniform dispersion of nanoparticles. Distilled water and a mixture with ethylene glycol (50%) was used as reference standards with TC and viscosity values of octadecane obtained from literature. Investigation of samples was performed using SEM and TEM to present micrographs as shown in the figures below. $MPSiO_2$ exhibited spherical morphology as presented in fig. 13 with an average particle size of 350 +/- 100 nm and pore size of around 5.0 nm [7].

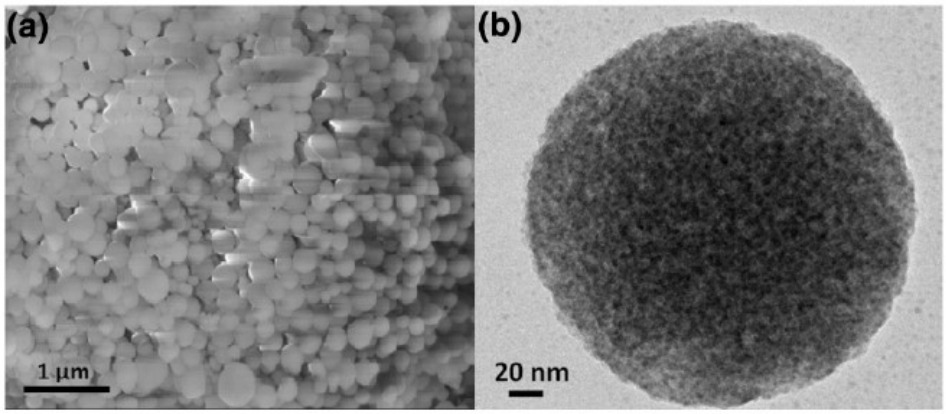

Fig. 13 SEM of $MPSiO_2$ particles [7]

Experiments were performed at different mass fractions of $MPSiO_2$ and temperature as indicated in the graphs of fig. 14. As seen from the graphs in fig. 14 the TC decreases with increase in temperature until the crystalline regions become unstable when the melting point is reached resulting in an increase in TC. This confirms that the TC decreases with increasing temperature and increases with further loading of nanoparticles. Rheological property investigation found that the PCM/$MPSiO_2$ behaves like a Newtonian fluid at all temperatures for $\varphi_m \leq 0.01$, however for higher loads of nanoparticles non-Newtonian behavior was observed. Viscosity will increase when the PCM is in a liquid state thus for 5% wt $MPSiO_2$/PCM this increase in viscosity was observed at 35 ^oC which corresponds to the melting point of the sample [7].

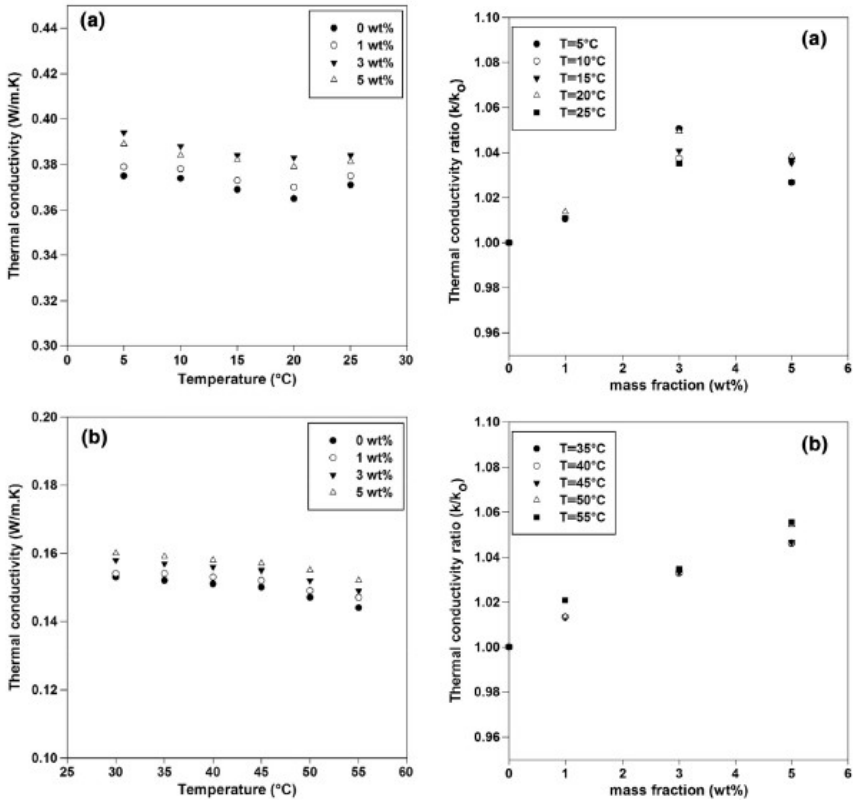

Fig. 14 SEM and TEM graphs of $MPSiO_2$ nanoparticle analysis [7]

As seen from the graphs in fig. 14 the TC decreases with increase in temperature until the crystalline regions become unstable when the melting point is reached resulting in an increase in TC. This confirms that the TC decreases with increasing temperature and increases with further loading of nanoparticles. Rheological property investigation found that the PCM/MPSiO$_2$ behaves like a Newtonian fluid at all temperatures for $\varphi_m \leq 0.01$, however for higher loads of nanoparticles non-Newtonian behavior was observed. Viscosity will increase when the PCM is in a liquid state thus for 5% wt MPSiO$_2$/PCM this increase in viscosity was observed at 35 ^oC which corresponds to the melting point of the sample [7].

Ho et al. [30] based the experiment described in their article on the same literature principles as described by Qian et al. [8], however the authors created a nanoparticle-embedded PCM which was prepared by an emulsion technique using a non-ionic surfactant to disperse alumina (Al_2O_3) nanoparticles in paraffin (n-octadecane). The materials effective thermophysical properties, including latent heat of fusion, density, dynamic viscosity, and thermal conductivity, were then investigated experimentally. Alumina nanoparticles were first coated with the non-ionic surfactant by a third of its mass fraction before dispersing the nanoparticles in paraffin using an ultrasonic disruptor for 3 h until full dispersion occurred. A constant temperature bath was used with temperature set above the melting point of the liquid paraffin. This technique was used to produce two samples of 5.0 wt% and 10.0 wt% alumina nanoparticles. The samples were then analysed using DSC measurement at a heating rate of 2 K/min and a temperature range of 20–40 °C with results illustrated in tab. 2 [30]. Density was measured using a hydrometer and the results illustrated in fig. 15.

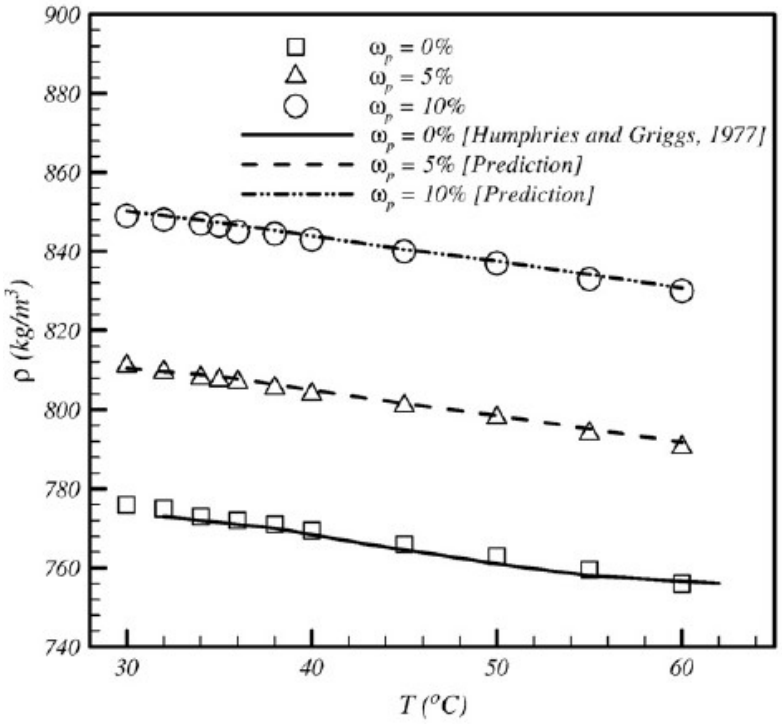

Fig. 15 Density results for alumina nanoparticles/paraffin PCM [30]

Table 2. DSC results for alumina nanoparticles/paraffin PCM [30]

Nanoparticle mass fraction ω_p	Melting temperature (°C)	Freezing temperature (°C)	Latent heat of fusion (kJ/kg)
0 wt.%	26.5	25.1	243.1
5 wt.%	26.0	25.0	225.6
10 wt.%	26.3	25.3	212.3

Values obtained compared well to literature as the density increased with an increased load of nanoparticles as expected. Thermal conductivity measurements are illustrated in fig. 16 [30].

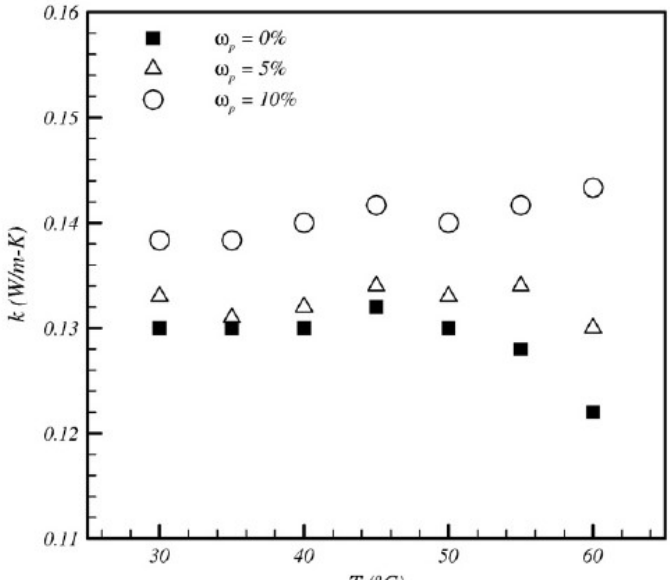

Fig. 16 Thermal conductivity results for alumina nanoparticles/paraffin PCM [30]

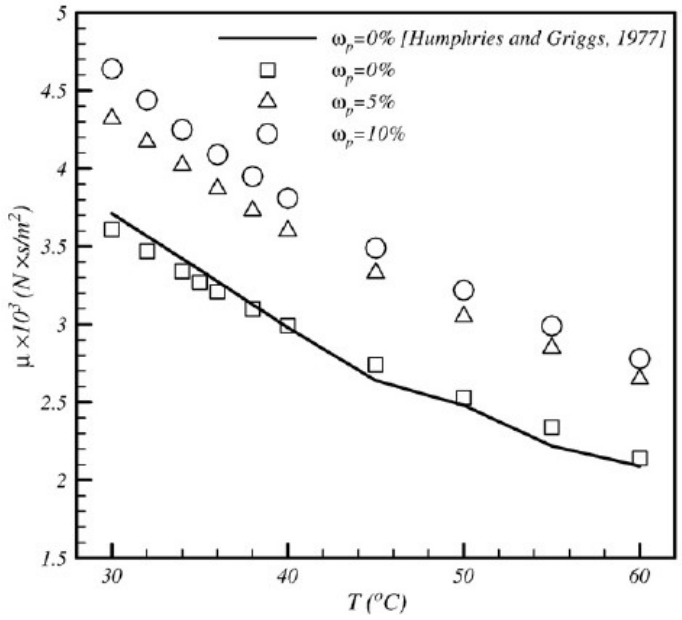

Fig. 17 Viscosity results for alumina nanoparticles/paraffin PCM [30]

Thermal conductivity of the 5 wt% and 10 wt% alumina nanoparticle samples were 2% and 6% higher respectively compared to that of the pure paraffin at 30 ºC. This result increases dramatically by up to 17% for the 10 wt% sample as the temperature increases to 60 ºC. This may be attributed to the enhanced Brownian motion of the nanoparticles within the base fluid as a result of reduced viscosity with an increase in temperature as depicted in fig. 17 for the viscosity measurements [30].
Viscosity results were as expected. At a temperature of 30 °C, relative increases of nearly 20% and more than 28% in the dynamic viscosity were found for 5 wt.% and 10 wt.% alumina nanoparticles samples respectively. This appeared about ten to four times greater than the relative enhancement in the thermal conductivity if compared at the same nanoparticle mass fractions respectively. It was therefore noted that with an increase in temperature as the viscosity of the solution decreases the thermal conductivity will increase correspondingly. Since the increase in viscosity was of greater magnitude than that of the increase of thermal conductivity for the respective samples reasonable doubt emerged given the efficacy for natural-convention-dominated thermal energy storage applications of the experiment [30].
Statements made in the article regarding the effects of nanoparticle concentration on the viscosity of a nanofluid is supported an article by Kang et al. [31] where a mathematical approach was taken using Einstein's relation to relate the effective volume fraction to the thermal conductivity of a nanoparticle solution. In the experiment conducted the thermal conductivity was predicted using this method for ultra-dispersed diamond powder in ethylene glycol, silver in water and silica in water. It was found that the thermal conductivity of the ethylene glycol solution was increased by up to 70 % for a 1 % UDD concentration with increases also noted for the silver and silica in water. The exact thermal conductivity could not be measured accurately due to the temperature uncertainty using the transient hot wire method [31].
For a reduction in thermal conductivity an article by Salaün et al. [5] for samples were prepared as illustrated in tab. 3.

Table 3. Composition of inner phase for preparation of microparticles [5]

Samples code	Core composition (wt.%)	Core content in particles	
		n-Alkane (wt.%)[a]	DSP (wt.%)[b]
ARD	*n*-Eicosane/*n*-hexadecane/tetraethyl orthosilicate 48/48/4	75.6	–
18	PVA-MDI/DSP nanoparticles 100	–	16.1
E2	*n*-Eicosane/(PVA-MDI/DSP) 68/32	68.1	3.6
H/E	*n*-Eicosane/*n*-hexadecane /(PVA-MDI/DSP) 34/34/32	72.0	4.4

[a] Determined by DSC.
[b] Calculated from EDAX analysis.

Sample ARD was prepared by microencapsulation of a ternary mixture of *n*-hexadecane, *n*-eicosane and tetraethyl orthosilicate in a 48/48/4 wt.% ratio. The in-situ polymerization occurred under constant stirring. Prior to the encapsulation, all three polymerization reactants were emulsified into an aqueous solution of Arkofix NM containing a binary mixture of Tween® 20 and Brij® 35 at pH 4 at 8000 rpm using ultra turrax high speed homogenizer. Following this the reaction was heated to 60 ºC with stirring at 400 rpm for 4 h until the end of the polycondensation reaction.

The pH of the solution was increased to 9 with 50 wt.% triethanolamine solution. The suspension was cooled to 25 ºC and filtered, followed by washing of the microcapsules twice with methanol and distilled water. Amino resin self-condensation around the core material droplet was linked due to surface activity that enriches the resin molecules within the interface. Hydrophilic/hydrophobic interactions of the partial methylolated melamine enhanced the concentration of the reactive resin molecules in the boundary layer. For this reason, the resin condensation proceeded at a much faster pace in the boundary layer than in the volume phase, which resulted in the formation of tougher microcapsule capsule walls [5].

Sample 18 was prepared by 4 g of DSP and 2 g of distilled water was mixed and added to a solution of 0.5 g of mixture of non-ionic surfactants of 1/3 of Span® 85 and 2/3 PEG 400 dioleate in 7 g of *n*-alkane as for the ARD sample to obtain the first solution. The solution was then stirred for 15 minutes at 9500 rpm whilst performing a reduction in droplet size by homogenizing the emulsion during the stirring. Similarly, emulsion 2 was prepared by homogenizing 8 g of 5 wt.% PVA solution in 8g of *n*-alkane. The particles in sample 18 were prepared by shearing under high speed for the two prepared emulsions with 3 g of MDI to crosslink the shell at 50 ºC for 30 min. The formed polymer nanoparticles were observed under SEM [5].

Preparation of samples E2 and H/E used the resultant solutions of sample 18 containing the nanoparticles in a paraffinic medium. This was emulsified in an aqueous solution containing 4 g of Tween® 20 in 100 g of distilled water and 9.2 g of Arkofix NM. 30 wt.%. Citric acid solution was used to reduce the pH to 3 whilst stirring at 8000 rpm under room temperature with an homogenizer. After 3 min, the reaction mixture was heated to 60 ºC, and stirring continued at 400 rpm for 4 hours using a blade stirrer until the end of the polycondensation. The microparticles were recovered by filtration and washed with methanol and distilled water followed by drying at room temperature overnight. From the two paraffinic solutions obtained in the preparation of sample E1 two types of multinuclear microparticles was obtained ‘E2’ and ‘H/E’, respectively [5].

Using SEM, the quality of the produced nanoparticles was investigated as illustrated in figures 18, 19 and 20.

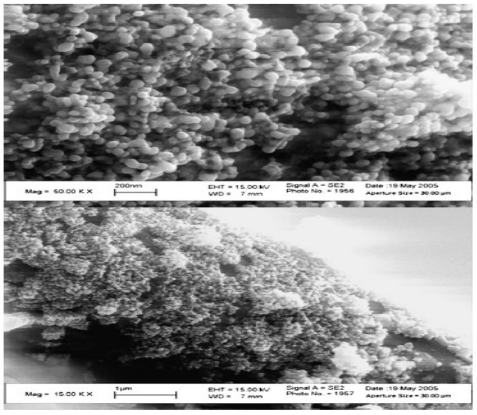

Fig. 18 SEM of sample E1 [5]

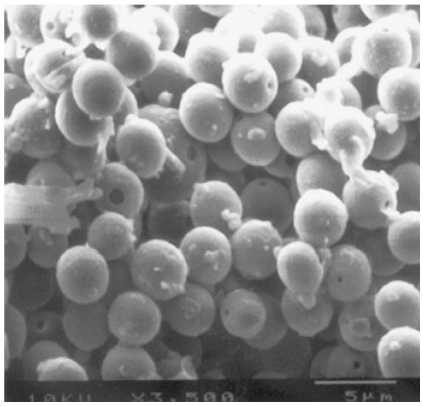

Fig. 19 SEM of ARD sample [5]

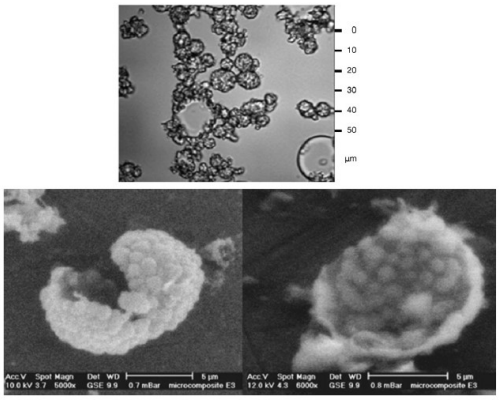

Fig. 20 SEM of sample E2 and a broken particle [5]

For the ARD sample the shell size ranged between 1-3 µm. For sample E1 polymer nanoparticles were produced with diameters of about 50 nm. Aggregation occurred due to high particle density. SEM analysis of sample E2 proved the high density and the configuration of polymer nanoparticles inside the shell. The shells included 68 % paraffin allowing the polymer nanoparticles to generate a very dense and thermally insulating structure as illustrated in figure 20 [5]. Fig. 21 indicates the DSC measurement for sample E2.

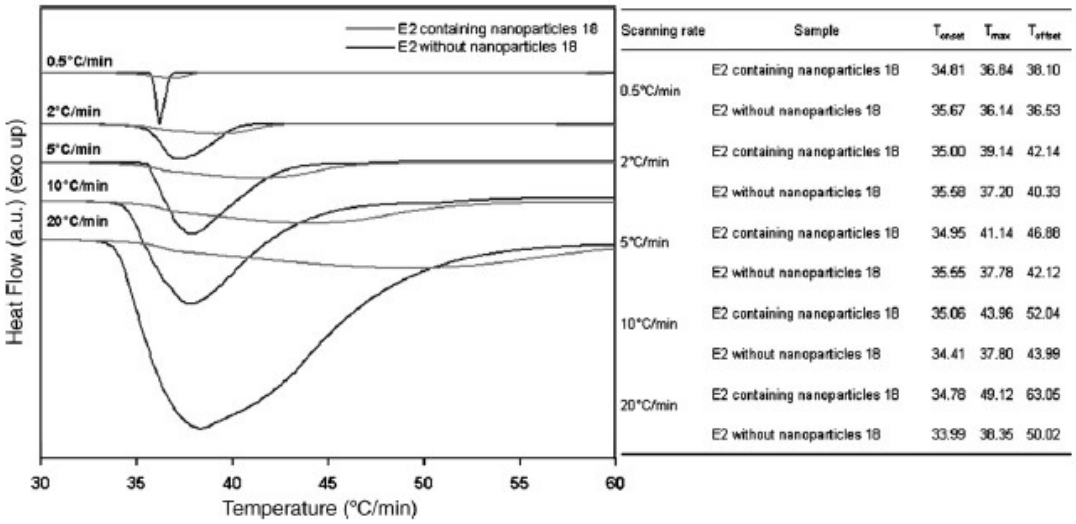

Scanning rate	Sample	T_{onset}	T_{max}	T_{offset}
0.5°C/min	E2 containing nanoparticles 18	34.81	36.84	38.10
	E2 without nanoparticles 18	35.67	36.14	36.53
2°C/min	E2 containing nanoparticles 18	35.00	39.14	42.14
	E2 without nanoparticles 18	35.58	37.20	40.33
5°C/min	E2 containing nanoparticles 18	34.95	41.14	46.88
	E2 without nanoparticles 18	35.55	37.78	42.12
10°C/min	E2 containing nanoparticles 18	35.06	43.96	52.04
	E2 without nanoparticles 18	34.41	37.80	43.99
20°C/min	E2 containing nanoparticles 18	34.78	49.12	63.05
	E2 without nanoparticles 18	33.99	38.35	50.02

Fig. 21 DSC for sample E2 [5]

The value of the latent heat was determined to be equal to 176 J/g. It was found that the temperature at which the solid-liquid transition started was the same, but the temperature span was 50% larger for the nanoparticles based PCM compared to the conventional microcapsules. This modification in the extended temperature span of the phase change is beneficial for textile application because the temperature will be maintained under a broader heat flux amplitude [5]. Thermal conductivity measurements for the samples ARD and E1 are presented in fig. 22.

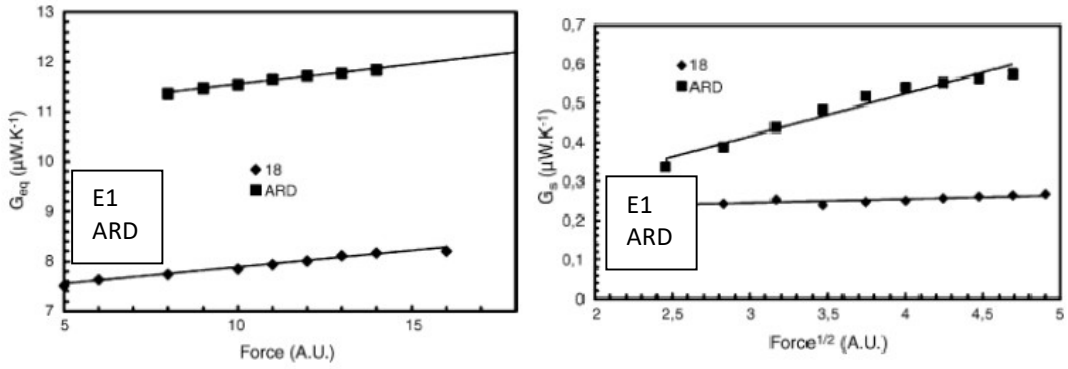

Fig. 22 Thermal conductivity measurements of samples ARD and E1 [5]

The ARD sample had a higher thermal conductivity than sample E1. As the graphs progress as a function of the electrical power in the probe, increases in the temperature resulted in both samples become more thermally resistive.
Since samples E2 and H/E are 60 % - 70 % more insulating than paraffin this confirmed the theory of insulating polymers such as the polymers used to result in a decrease in thermal conductivity [5].

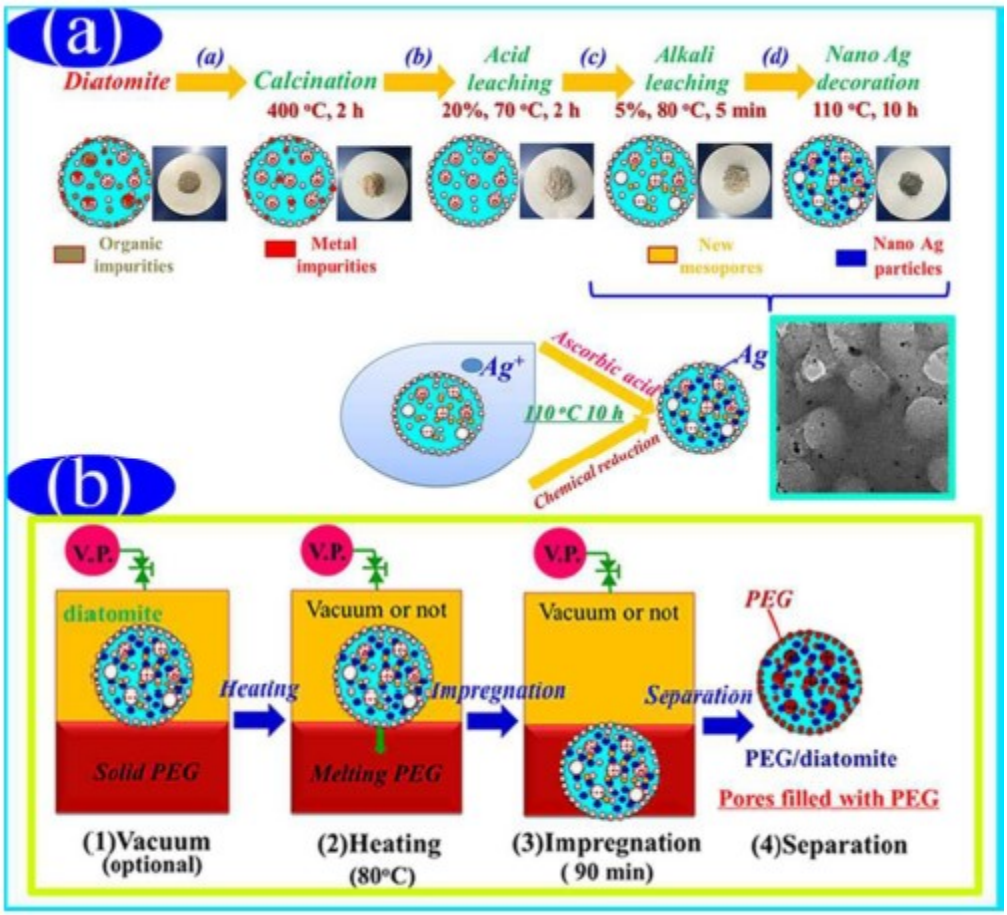

Fig. 23 Purification process of diatomite and impregnation [8]

Experimental procedure from the article by Qian et al. [8] used raw diatomite purified by the process as illustrated in fig. 23(a) below. Incorporation of the AgNPs in the later stage of the process. AgNPs were produced by the chemical reduction of silver nitrate. Analytical grade polyethylene glycol (MW = 4000) was used.
Fig. 23(b) illustrates the process in which way the PEG/DtAg ss-PCMs were obtained [8].
Results for the purification of the diatomite are presented by the SEM images in fig. 24, where (a) illustrates the disc and cylindrical like structures of the raw diatomite powder. This also indicates the impurities blocking the pores. (b) After acid treatment some of the impurities were removed. (c) Morphology of the porous structure is maintained after alkali leaching. (d) Enlargement of (c) indicating where the PEG will disperse the AgNPs in the pores of the purified diatomite. (e) & (f) indicates the deposit of the AgNPs on the surface of the structure. The energy dispersive X-ray spectroscopy spectrum confirms the presence of Silicon, Oxygen and Silver in the composite while proper AgNP dispersion was confirmed visually [8].

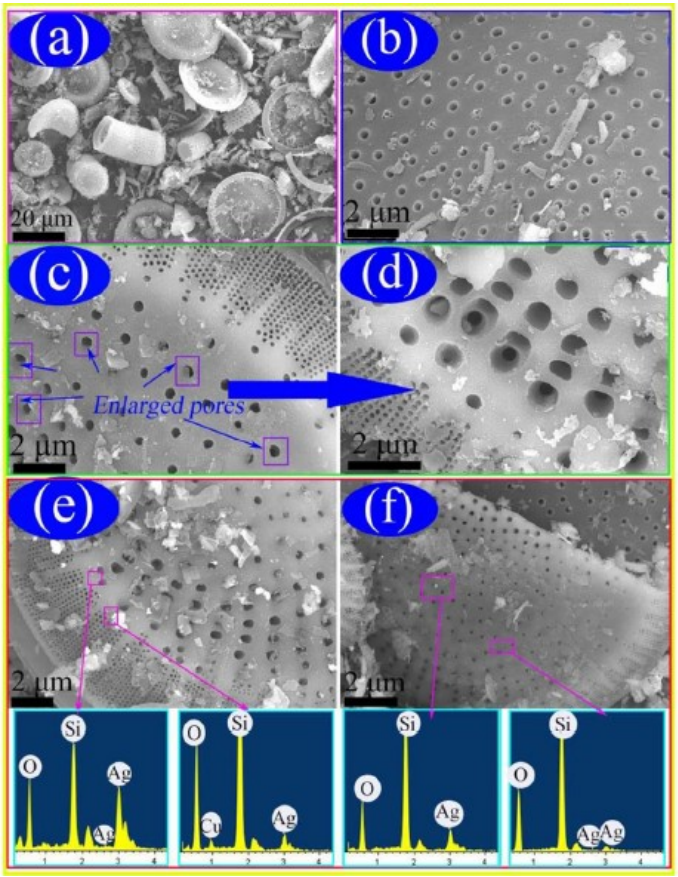

Fig. 24 SEM analysis [8]

This was also confirmed with TEM image analysis as in fig. 25. It corresponds with the observations made during SEM analysis.

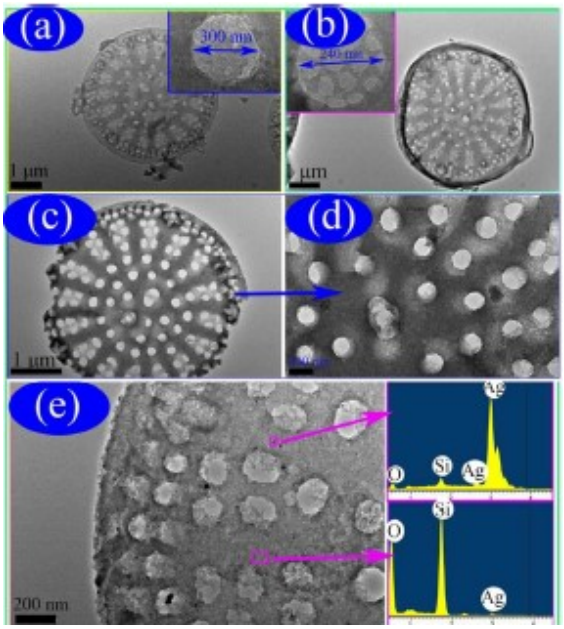

Fig. 25 TEM analysis [8]

X-ray diffraction results indicated that the PEG crystal structure was not destroyed after impregnation as well as high sample purity obtained since no deviations from the expected graph pattern was observed. FTIR spectra confirmed the silver in the composite was in pure form and that there was no chemical interaction between the PEG and DtAg. Fig. 26 shows that PEG with different mass ratios (30 %, 40 %, 50 %, and 63 %) was well dispersed in the porous structure of the DtAg.

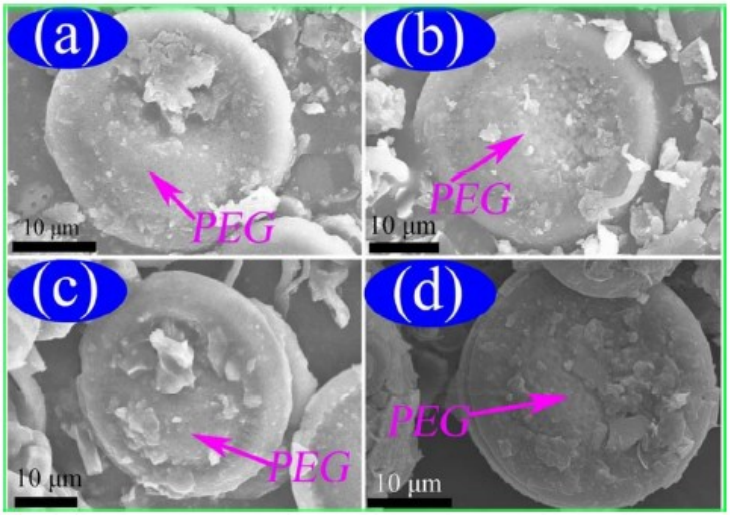

Fig. 26 SEM analysis of prepared PEG/DtAg ss-PCMs [8]

The multi-porous structure of the diatomite prevented liquids and PEG leakage because of capillary action and surface tension forces. As indicated in figure 26(d), PEG was not leaked from the surface of the composite when the PEG was in the melting state because the hot spot made by the electric beam made the investigated PCM locally melt when conducting SEM. From this the maximum appropriate mass ratio of the PEG in the composites was determined to be 63 % [8].

Thermal behavior of the samples was measured using DSC and the data obtained for the respective samples is presented in tab. 4.

Table 4. DSC results of different PEG/DtAg ss-PCM samples [8]

Samples	PEG Mass Ratio (wt%)	Melting Process		Solidifying Process	
		H_M(J/g)	T_M(°C)	H_S(J/g)	T_S(°C)
PEG PCM	100	180.3	60.51	164.6	38.5
ss-PCM1	30	51.5	59.21	46.1	38.63
ss-PCM2	40	70.2	58.86	64.1	39.21
ss-PCM3	50	88.4	59.13	80.3	40.54
ss-PCM4	63	111.3	59.45	102.4	41.02
ss-PCM5	63	110.7	59.83	103.3	39.54

Thermal conductivity was measured using a hot disk thermal constant analyser at room temperature. Results are illustrated in fig. 27.

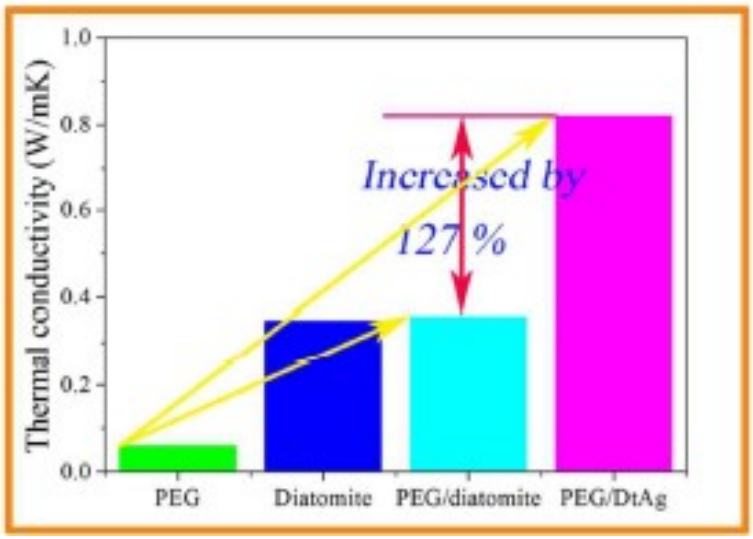

Fig. 27 Thermal conductivity results [8]

This provided an improvement of 127% for the composite PCM compared to raw diatomite using the process discussed. This was due to the improved thermal conductivity if the purified diatomite as well as the high thermal conductivity of the silver [8].

XRD, FTIR, TGA and a 200-cycle test results proved the excellent chemical compatibility and the improved super cooling extent, stability, and reliability of the created PEG/DtAg ss-PCMs [8].

2.2 Silver Nanoparticles

Xue et al. [11] coated nanofibers with silver nanoparticles to incorporate an antimicrobial effect onto the textile whilst also modifying the nanoparticles to promote hydrophobicity. The process of application of the nanoparticles to the fibres are presented in figure 28 below. Silver nitrate was used to form the nanoparticles as this proved to be one of the most common methods in literature.

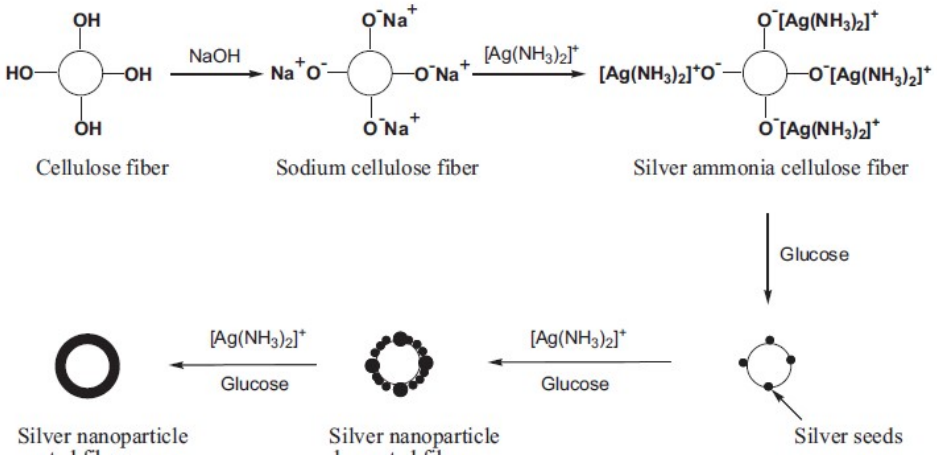

Fig. 28 Formation of nanoparticle coated fibers [11]

According to the scheme above, the cotton textiles were treated with 10% aqueous NaOH solution at room temperature for 10 minutes followed by rinsing with distilled water. 28% Aqua ammonia was added dropwise to 0.5 M silver nitrate solution until the solution turned colorless forming $[Ag(NH_3)_2]^+$.

The alkali treated cotton textile was added to the formed colorless solution and allowed to react for 1h followed by transfer to a 0.1 M glucose stock solution for 5 minutes. The residual $[Ag(NH_3)_2]^+$ was added to the textile in the glucose solution and reaction occurred for 15 minutes after which the textile was removed and rinsed and allowed to dry in air. The samples were then hydrophobized with 3% HDTMS in ethanol for 1 hour at 80 ^oC and cured at 130 ^oC for 1 hour [11].

Bacterial tests were conducted by the bacterial resistance ring method and the reduction of bacterial growth test. Both tests are standardized. The possibility of electrical conductivity incorporated in the fibre modification was measured as the resistance between two points on the original cotton sample and the modified sample [11].

SEM results of the modified fibers as well as the contact angle of water to the modified textile is presented in fig. 29 [11].

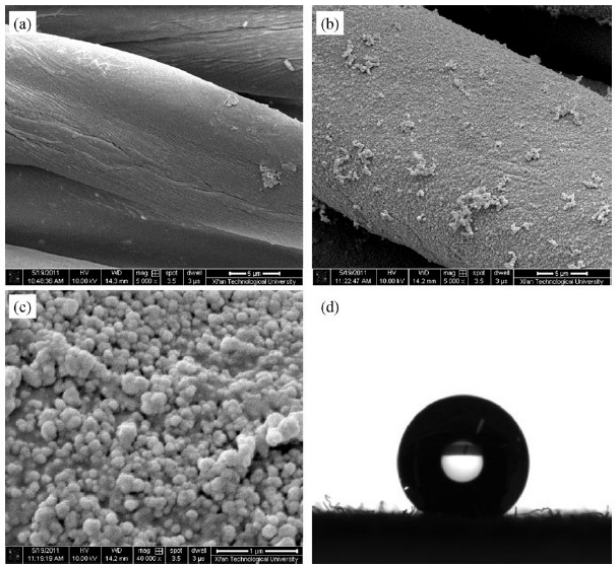

Fig. 29 SEM images of (a) original cotton fiber, (b) silver nanoparticle coated cotton fiber, (c) magnification of (b), (d) water droplet contact angle with textile [11]

From the SEM image it is clear that the fibers were sufficiently coated with silver nanoparticles. The water contact angle was determined to be 157.3° for the 5 µl droplet applied to the textile surface. XRD confirmed the presence of pure silver nanoparticles as no impurities were observed in the diagram. The electrical resistance of the textile was very low at 37.0 Ω compared to the infinite result of the original sample which is unable to conduct electricity. The antimicrobial activity was confirmed to destroy 99.99 % of bacterial colonies with an inhibition area of 8.78 mm, however this could possibly be higher as the hydrophobic treatment could potentially inhibit the release of silver ions. The modified textile maintained this property after 10 wash cycles [11].

2.3 Conductive Nanoparticles

Fabrication of the conductive flexible material described by Park et al. [12] followed the scheme as illustrated below in fig. 30. This process can be described a follow: (a) presents the non-woven mat of SBS rubber collected on a surface treated silicon wafer which was peeled off afterwards. This was then dipped into the silver precursor solution of $AgCF_3COO$/ethanol. Both precursor and solvent are absorbed by the fibers with the formation of silver shells on the surface of the fibers which can break under strain, however conductivity is maintained by percolation of the silver nanoparticles inside the fibers as well as bridges formed by the debris of the broken shells. The silver nanoparticle solution was nozzle printed onto the SBS electro spun mat. Absorption of the silver nanoparticles is promoted by the ion-dipole interaction between the hydroxyl groups of the alcohol and the trifluoroacetate anions. This causes the fibers to swell as indicated in fig. 30 (b) until saturation occurs at 15 wt.% concentration. The saturated mat retained 62 wt % silver content after chemical reduction. FTIR spectroscopy confirmed the presence of precursor inside the fibers

which prevented the fibers from shrinking back to dimensions obtained before spinning as indicated by fig. 30 (c) [12].

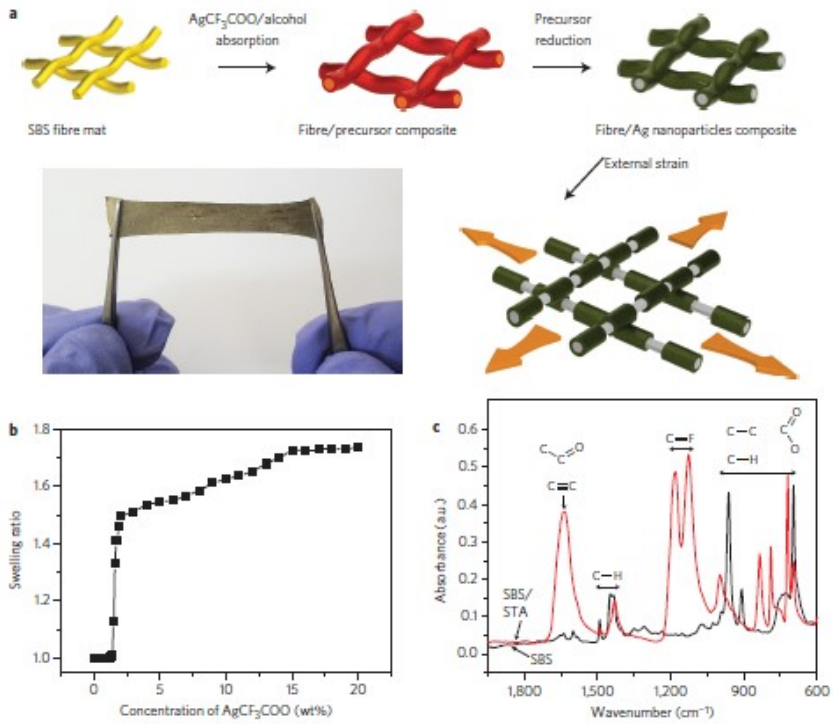

Fig. 30 Formation of SBS rubber impregnated with silver nanoparticles [12].

From the graph in fig. 31 (a) presented above depicts the stretch stain vs conductivity of the material.

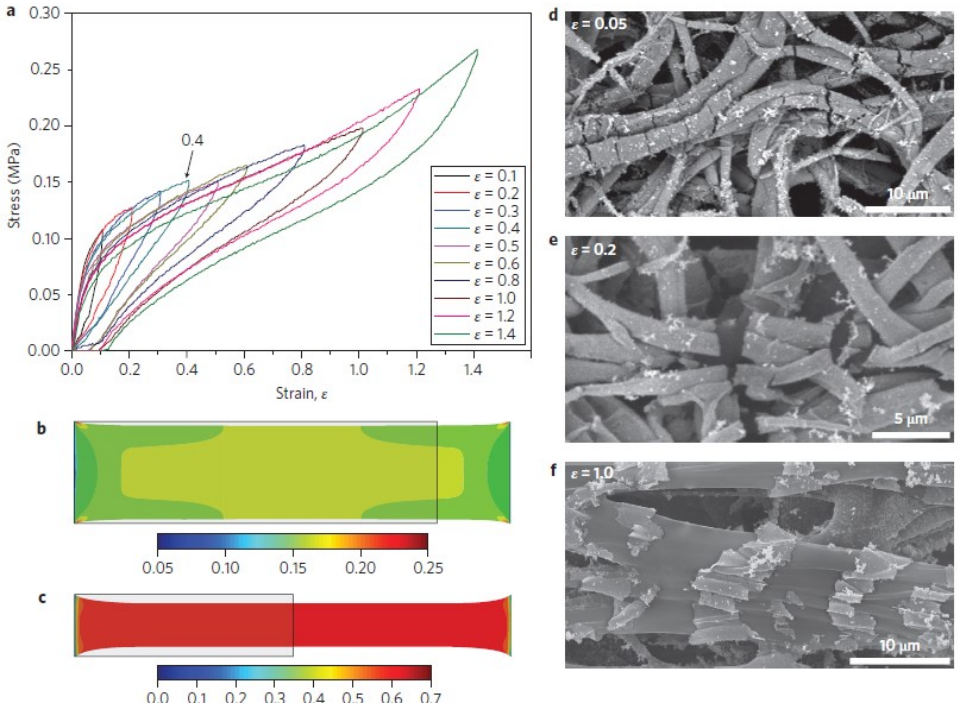

Fig. 31 Stress strain vs conductivity (a), (b) & (c) color coded graph of applied stress strain with SEM images at respective strain values (d)-(f) [12]

It was noted that under low stress the conductivity was barely influenced and returned to normal upon relaxation of the fibers. However, upon excessive stretching to the yield point of the SBS fibers the conductivity decreased significantly, adopting a new conductivity value upon release corresponding to that attained under the maximum stretch. It is also possible to form a circuit on the mat using the nozzle printing technique [12]. From the graph in fig. 31 (a) presented above depicts the stretch stain vs conductivity of the material. It was noted that under low stress the conductivity was barely influenced and returned to normal upon relaxation of the fibers. However, upon excessive stretching to the yield point of the SBS fibers the conductivity decreased significantly, adopting a new conductivity value upon release corresponding to that attained under the maximum stretch. It is also possible to form a circuit on the mat using the nozzle printing technique [12]. One of the high performance thermoelectric materials investigated by the authors in the article by Li et al. [13] were Bi_2Te_3 alloys where it was found that by mechanical milling of the bulk material into a nano powder resulted in an increase in the ZT-value of $Bi_2Sb_{2-x}Te_3$ to obtain a value of ZT=1.4 at 373 K.

This was attributed to a decrease in thermal conductivity by larger scattering at the grain boundary and the presence of nanoparticles. Also investigated was the development of a melt–quench–anneal–spark plasma sintering method to form bulk nanostructural p-type $Bi_{0.52}Sb_{1.48}Te_3$ with a ZT-value of 1.56 at 300 K. Also obtained was a maximum ZT =1.47 at 438 K for Bi_2Te_3/Sb_2Te_3 bulk nanocomposites with laminated nanostructures using hydrothermal synthesis and hot pressing. A 20% increase in the ZT-value was obtained by the incorporation of SiC nanoparticles into the Bi_2Te_3 alloy at 0.2 volume percent, however further addition resulted in a decrease of the ZT value since the SiC particles has a higher electrical resistivity and thermal conductivity than that of the alloy. An increase in micro hardness and fracture toughness was observed and improved the ability to handle and manufacture the composite material [13].

$CoSb_3$ based skutterudites were also investigated due to the compound's high effective mass and carrier mobility. The compound has a very high thermal conductivity of 10 W m^{-1} K^{-1} compared to that of Bi_2Te_3 (1.0-1.5 W m^{-1} K^{-1}) which prevents it from competing. This is overcome by incorporating a smaller filler elemental ion, such as iron, inside the cage-like structure formed at the center of the parent compound which was able to reduce the thermal conductivity to 1.4 W m^{-1} K^{-1}. This is due to the inserted ion rattling at the equilibrium position generating a significant number of phonons. It is found that the filler elemental ion with the largest cage filing fraction resulted in the largest increase in ZT-values. Only filler elements with electro negativities larger than 0.8 was able to enter the cage-like structure of the central metal atom in the compound. It was also state that a good thermoelectric device requires both n- and p-type legs to overcome possible failure die to thermal stresses making $CoSb_3$ an excellent choice for medium temperature applications due to the incorporation of both components [13].

$Ag_{1-x}Pb_{18}SbTe_{20}$ was successfully synthesized and possessed a NaCl symmetry structure with nanoparticles scattered in the PbTe matrix. This proved to have a very

high ZT-value of 2.2 at 800 K making this an excellent thermoelectrical material. The study found that the thermoelectrical materials are very sensitive to chemical composition especially with regards to lead content. With the use of an annealing treatment to the thermoelectrical material great success had been achieved in reducing the thermal conductivity of the material whilst simultaneously increasing the electrical conductivity as the treatment assists in the formation of a nanostructure which favors electron transport and phonon scattering. This resulted in a significant improvement of the ZT-value to 1.7 at 703 K. The compound was also resynthesized to provide a low thermal conductivity value of 0.3 W m^{-1} K^{-1} and ZT-value of 1.59 at 673 K. Comparable values were obtained by substituting silver for potassium and sodium with slight deviations in ZT-values and temperature [13].

Half-Heusler compounds prove to be more environmentally friendly compared to compounds containing lead with symmetry that can be interpreted as two interpenetrating cubic face-cantered-cubic motifs with an embedded cubic motif at the center of the structure. The chemical structure of these compounds are typically MgAgAs type systems. These compounds typically have high thermal conductivity values resulting a lower ZT-value compared to previously mentioned compounds [13].

Oxide materials such as with the discovery of $NaCo_2O_4$ usually have a high thermal stability and oxidation resistance which makes them good for use in high temperature applications. Previously these materials have been ignored due to low electrical conductivity but have gained new interest with recent discovery of $NaCo_2O_4$. This material possesses a similar structure to the superconductor YBaCuO sandwiched between a CoO_2 and sodium layer which forms laminated sheets on the outside surfaces. $NaCo_2O_4$ has an unusually large Seebeck coefficient as a result of strong electronic correlation effect in the material. Coupled with a high electrical conductivity the power factor of the thermoelectric material is 5000 W m^{-1} K^{-1} which is higher than that of previously mentioned Bi_2Te_3 (4000 W m^{-1} K^{-1}) [13].

Dermanaki Farahani et al. [17] used synthesized silver nanoparticles and purchased for samples indicated in tab. 5.

Table 5. Silver nanoparticle ink composition and samples [17]

Coating materials	Materials used	Proportion [wt%]	Synthesized or purchased conductive fillers
PEDOT:PSS	Ag1-ink	50	Synthesized
Binary nanocomposite	PEDOT:PSS	50	Heraeus
	Ag2-ink	50	Synthesized
	PEDOT:PSS	50	Heraeus
Epoxy-blended PEDOT:PSS	Ag1-ink	50	Synthesized
Ternary nanocomposite	PEDOT:PSS	10	Heraeus
(biphasic)	EPI-REZ 5522-WY-55/Epikure 8290-Y-60	40	Momentive chemicals
	Ag2-ink	50	Synthesized
	PEDOT:PSS	10	Heraeus
	EPI-REZ 5522-WY-55/Epikure 8290-Y-60	40	Momentive chemicals

Two different nanocomposite materials were produced as illustrated in table 5 above and their compositions within the nanocomposites listed under materials used. The

binary nanocomposite was a blend of the conductive silver nanoparticle inks and PEDOT:PSS as a conductive binder. For 50 wt.% of ink, the desired amount of the mixed conductive ink was dissolved in 10 mL deionized water with sonication for 30 min. The solution was then added to a specific amount (1:1 ink to PEDOT:PSS) of PEDOT:PSS in a 100 mL glass bottle and ultra-sonicated for 30 min. This was followed by stirring at 400 RPM for 3 hours. The ternary nanocomposite was an 80:20 blend of epoxy emulsion with PEDOT:PSS and the conductive silver nanoparticle inks. The epoxy emulsion formed was added to the mixture of PEDOT:PSS and the silver inks for improvement of the mechanical resistance of the final coatings. The final nanocomposite contained 50% of the ink which was first solubilized in 10 ml distilled water with ultra-sonication for 30 min. The solution was then added to a weighted 80:20 amount of the epoxy emulsion and PEDOT:PSS. This was followed by stirring at 80 ºC for 3 hours at 400 rpm. These inks were applied to aerospace grade carbon fiber sheets [17]. The process of application is illustrated in fig. 32.

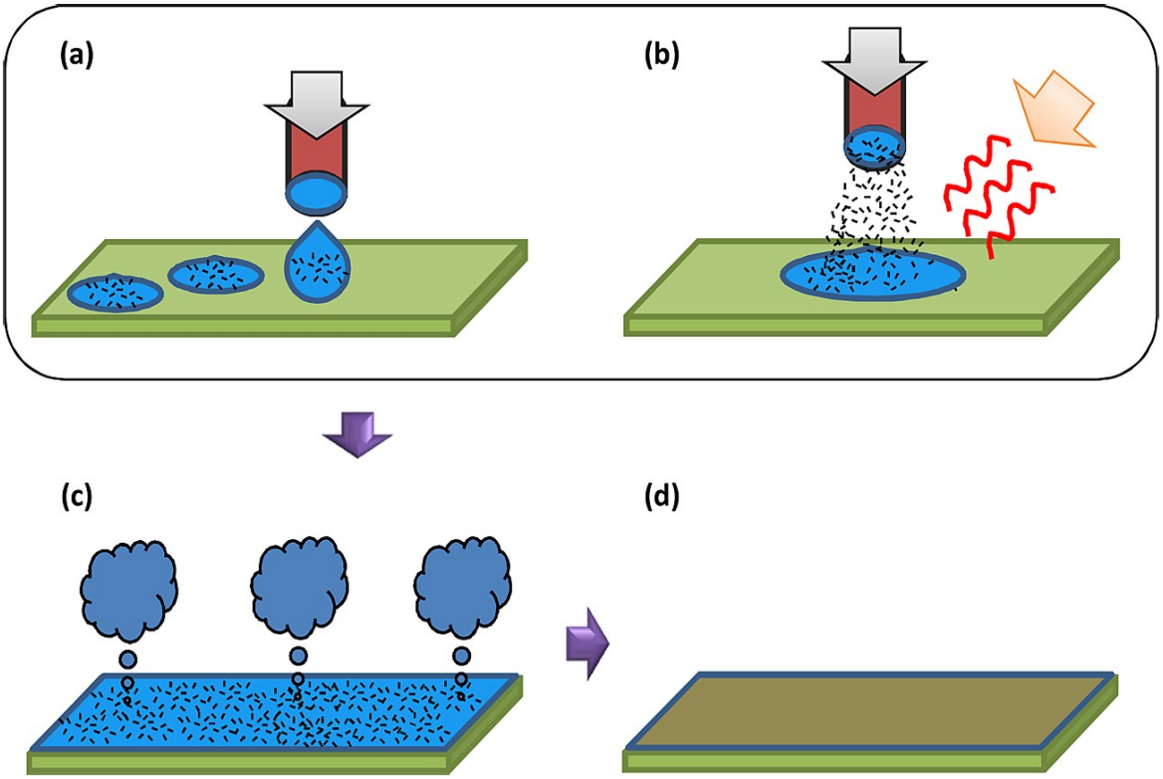

Fig. 32 Application process of the two ink types either by spray or coating sheets [17]

Two different methods of coating application were used namely spraying and casting for each of the conductive ink samples. After application the coated samples were dried at 90 ºC for 20 minutes at 0.15 bar pressure.

For both application methods thermal annealing of the coating materials was performed at 140,180, and 200 ºC. Fig. 33 (a) shows the coated material versus the sample before coating whilst (b) illustrates the cross section of the coated materials with magnification (c) & (d) [17].

The coating density was determined to be 4200 kg m^{-3} and 4600 kg m^{-3} for the binary and ternary samples respectively which was much lower than the density of the silver inks used which had a density of 7000-8000 kg m^{-3}. The densities obtained are lower than that of copper foils currently used in the aerospace industry.

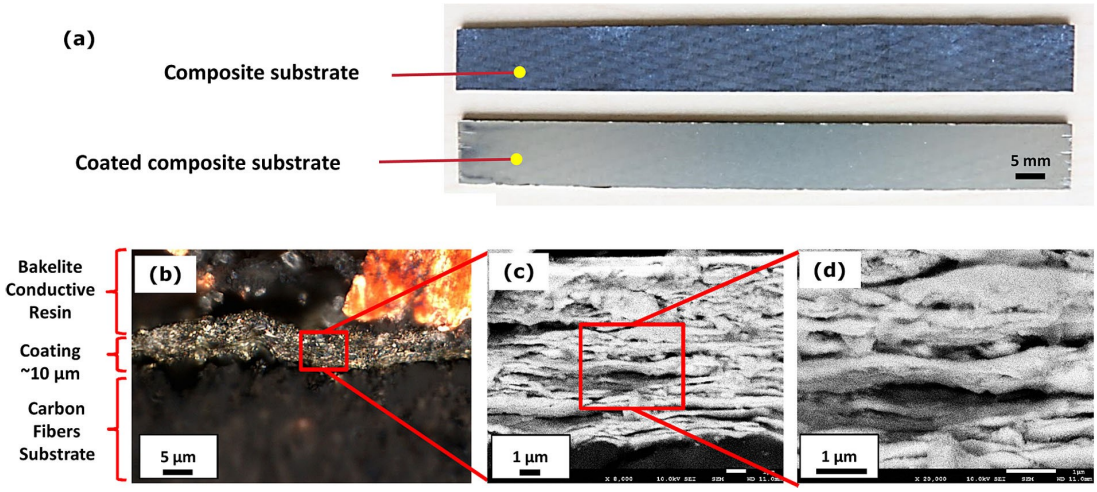

Fig. 33 (a) Sample before and after coating, (b) Cross sectional view with magnification (c) & (d) [17]

Fig. 34 indicates the effects of different annealing temperatures for the respective samples. It was hypothesized that with increased annealing temperature the coatings attained a connecting feature and resulting in a smoother surface above 140 ºC.

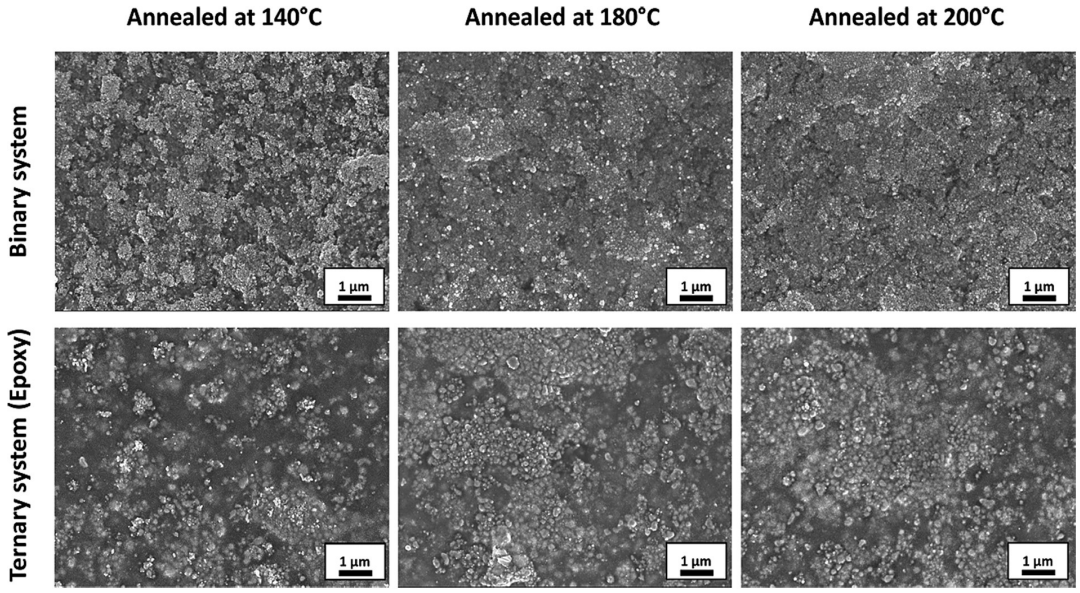

Fig. 34 Optical images of samples annealed at different temperatures [17]

It was thus hypothesized by the authors that the higher annealing temperature results in densification of the applied ink, however measurement results were within the margin of error. Impurities were observed for the Ag ink samples as sintering occurred during annealing. For adequate removal of impurities annealing temperatures of above 250 ºC are required to improve the electrical conductivity;

however, cracks were observed by the authors at temperatures above 220 ºC [17]. Mechanical and electrical conductivity properties are presented in tab. 6.

Table 6. Mechanical and electrical conductivity results for binary and ternary samples with respective ink types [17]

Materials	Hardness [MPa]	Modulus [GPa]	Specific resistivity [Ω g cm^{-2}] Non-annealed	Annealed at 140 °C	Annealed at 180 °C	Annealed at 200 °C
Ag1-ink – binary system	350 ± 20	6 ± 0.4	$1.8 \pm 0.3 \times 10^{3}$	$2.3 \pm 0.5 \times 10^{0}$	$5 \pm 0.1 \times 10^{-2}$	$4.2 \pm 0.3 \times 10^{-3}$
Ag1-ink – ternary system	385 ± 15	8 ± 0.3	$5.1 \pm 0.05 \times 10^{1}$	$9.9 \pm 0.1 \times 10^{0}$	$4.5 \pm 0.5 \times 10^{0}$	$3.4 \pm 0.07 \times 10^{0}$
Ag2-ink – binary system	320 ± 25	5 ± 0.3	$8.7 \pm 0.02 \times 10^{1}$	$7 \pm 1 \times 10^{-1}$	$1 \pm 0.5 \times 10^{-1}$	$2 \pm 0.9 \times 10^{-1}$
Ag2-ink – ternary system	350 ± 12	8 ± 0.5	$2.9 \pm 0.07 \times 10^{2}$	$7.3 \pm 1 \times 10^{0}$	$2 \pm 1 \times 10^{-1}$	$2.7 \pm 0.1 \times 10^{-1}$

Slightly higher values for the hardness and modulus were observed for the ternary system versus the binary system which could be attributed to remaining epoxy in the samples. Tab. 7 illustrates the effectiveness of the nanoparticle polymer binding to the substrate with the spray technique being the preferred method of application.

Table 7. Comparison of spray vs casting application methods [17]

Materials/Coating methods	Specific resistivity [Ω g cm^{-2}]	Adhesion grade 0B (poor) –5B (best)
Binary system/Casting	$6.4 \pm 0.3 \times 10^{-1}$	Test not performed: flaky/bad adhesion/peeling
Ternary system/Casting	$7.1 \pm 0.8 \times 10^{2}$	Test not performed: flaky/bad adhesion/peeling
Binary system/Spraying	$4.2 \pm 0.3 \times 10^{-3}$	5B
Ternary system/Spraying	$3.4 \pm 0.07 \times 10^{0}$	5B

It was noted that with increasing annealing temperature nanoparticle polymer binding did become more effective for the casting method, however only when annealed at 180 ºC and above compared to the spray method which showed good binding results from 140 ºC [17].

Electrical conductivity of the samples improved with annealing temperature; however, the binary samples indicated the highest electrical conductivity as lowest resistivity as seen in fig. 35.

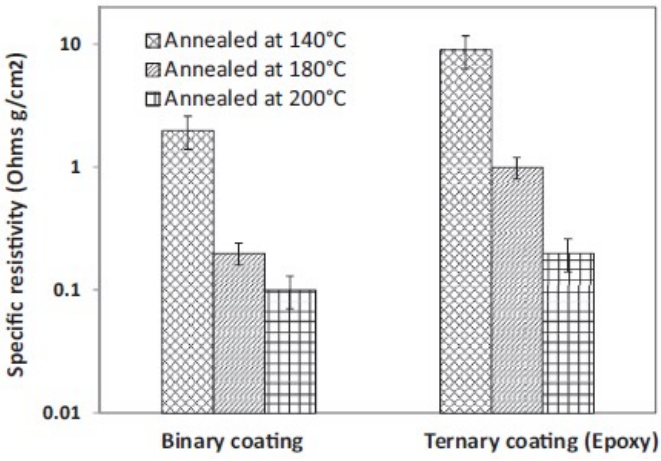

Fig. 35 Electrical resistivity measurements for the binary and ternary systems [17]

This proved that higher annealing temperature is preferred to increase the electrical conductivity of the nanoparticle polymer which was determined to be 1.8 +/- 0.3 10^{3}

Ω g cm^{-2} at 140 ºC which increased to 4.2 +/- 0.3 10^{-3} Ω g cm^{-2} when annealed at 200 ºC [17].
Los et al. [16] investigated various filler materials to reflect or absorb electromagnetic radiation at 1-2 GHz with a split post dielectric resonator. This is a typical range for every day devices used by consumers [16]. Results of these are presented in tab. 8.

Table 8. Electromagnetic interference shielding effectiveness of composites with various fillers in a polyether sulfone matrix at a sample thickness of 2.8 mm [16]

Filler	Vol, %	EMI shielding effectiveness, dB
Al flakes (15 x 15 x 0.5 mm)	20	26
Steel fiber (1.6 mm dia. x 30–56 mm)	20	42
Carbon fiber (10 mm dia. x 400 mm)	20	19
Ni particles (1–5 mm dia.)	9.4	23
Ni fibers (20 mm dia. x 1 mm)	19	5
Ni fibers (2 mm dia. x 2 mm)	7	58
Carbon filaments (0.1 mm dia. x >100 mm)	7	32
Ni filaments (0.4 mm dia. x >100 mm)	7	87

The use of mainly metals as fillers resulted in results mainly focused on electromagnetic radiation reflection rather than absorption. The best results were obtained using Nickel fibers with the highest effectiveness observed. It was also noted that the use of metal flakes/wires can be treated with methanol to improve corrosion resistance. The ICRI developed and patented an electrochemical method for manufacturing of the metal fillers which improved production costs significantly [16].

2.4 Fiber Reinforced Composites with Conductive Nanoparticles

Materials used by Böger et al. [18] included epoxy resin, anhydride hardener, imidazole accelerator and the addition of 0.3 wt % of carbon nanoparticles. Three forms of carbon nanoparticles were investigated in this experiment namely double wall carbon nanotubes, carbon black and multi walled carbon nanotubes. The modified epoxy system was used to manufacture glass-fiber laminates. Nanoparticles were dispersed in the resin by mixing without the addition of hardener or accelerator and passed through a three-roller mill. The collected resin was bottled and stored at a low temperature to prevent the agglomeration of the different carbon nanoparticles. The epoxy/carbon suspension was then mixed with hardener and accelerator using a laboratory vacuum stirrer. It was important that no air bubbles were formed in the matrix during this step. The additions to the epoxy will increased the viscosity

therefore heating to 45 ºC was necessary to compensate. Two glass fiber non-crimp fabrics were used on both sides of the epoxy resin to achieve the desired laminate with a stacking ration stated as (0º, +45º, 90º, -45º, +45º, 90º, -45º, 0º). Heating of the mould was kept at 45 ºC to ensure the viscosity of the epoxy matrix remained low for the injection process.

During processing an electrical field with a field strength of 33 V/cm was applied to the formed material in the z direction for orientation of the carbon nanoparticles to form a conductive network in the matrix. Curing occurred at 80 ºC for 4 hours and specimens were cut according to industry specification. Two tabs of two +-45º GFRP, 1 mm thick sheets were placed on the side of the specimens and on the fixture side, two tabs consisting aluminum. Post curing occurred for 8 hours at 140 ºC and contacted with conductive silver paint on the top and bottom sections of the sheet in the z-direction for conductivity measurement. The painted sides were polished to avoid possible short circuiting. For resistance measurement two opposite sides of the samples were painted with conductive silver paint, whereas for measurement in the z-direction the upper and lower surface of the test specimens were coated with conductive silver paint. For the tensile test specimen only a 15 mm wide electrode was applied to both sides in the center of the test specimens [18]. Both setups are presented in fig. 36.

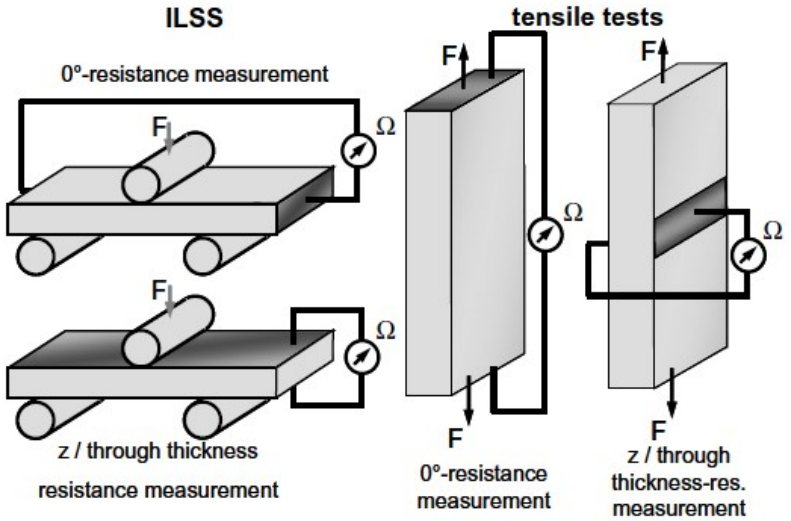

Fig. 36 Resistance and tensile test measurement setup [18]

Mechanical property testing involved the inter laminar shear strength, incremental tensile and the dynamic tensile tests. During mechanical testing the resistance was measured by applying a voltage to the specimens [18].
Interlaminar sheer stress results are presented in figs. 37, 38 and 39.

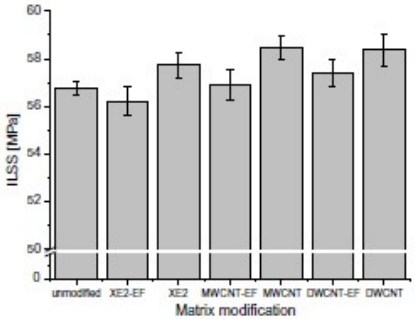

Fig. 37 Interlaminar shear stresses of the modified GF-NCF-EP materials [18]

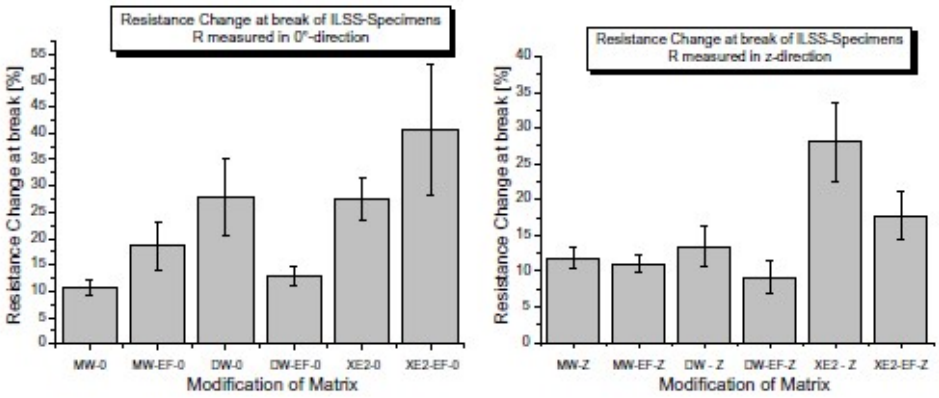

Fig. 38 Resistance at break measurement [18]

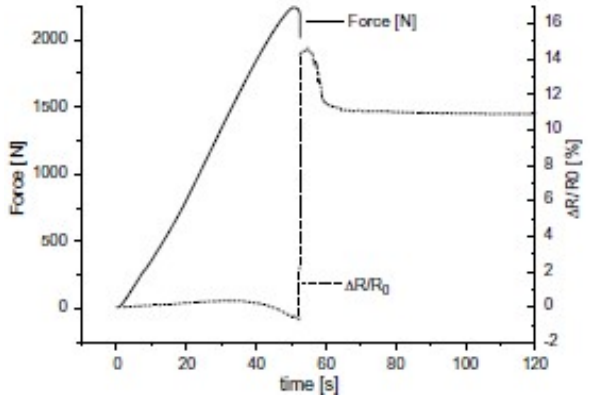

Fig. 39 Progression of force and resistance change during ILSS test [18]

As seen from the results in figs 37, 38 and 39 it is shown that the carbon-black modified epoxy laminates exhibited values of approximately 25–45 %, approximately 10–15 % for the nanotube-modified laminates and approximately 20–40 % for the carbon black modified laminates during the resistance change measured in z-direction. The authors contributed the abrupt increase in electrical resistance during measurement to be attributed to the interruption of electrically conductive pathways in the materials by delamination. Delamination, which occurs in the fiber plane which is orthogonal to the z-direction, could have been detected electrically in both

measurement directions (0^o- and z-direction). Two reasons explaining this phenomenon is first that the delamination was never a purely in-situ failure, but also propagating in thickness. Second, the electrical pathways formed by the nanoparticles are randomly 3D oriented in the laminates. Therefore, a resistivity measurement in the 0^o -direction is also affected by a delamination in the fiber plane, since the electrical pathways are partly oriented in z-direction. Fig. 39 shows that for measurement in the z-direction the resistance was almost unaffected by the application of sheer forces [18].

The effect of resistance during repeated stress was measured as illustrated in fig. 40 and the percentage resistance change indicated in graph (b) of the same figure. It is noted that after the 5^{th} cycle residual strain was observed.

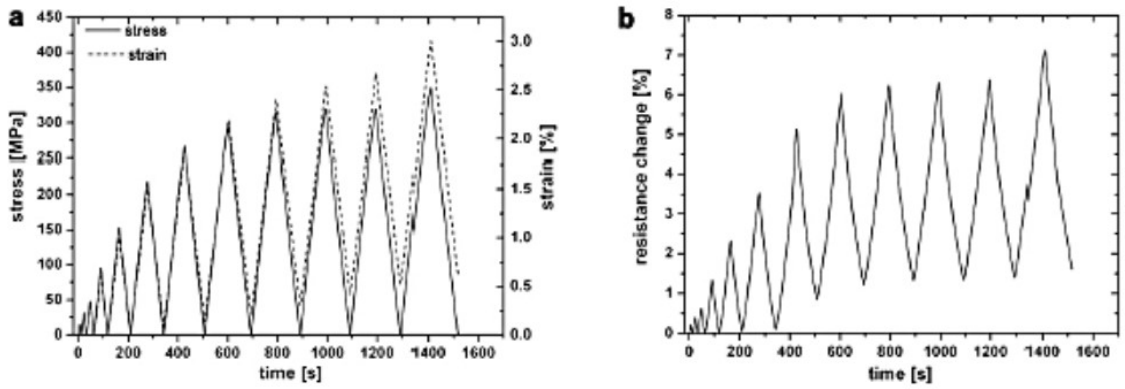

Fig. 40 (a) Repeated stress strain vs time, (b) Percentage resistance change vs time [18]

Fig. 41 indicates the effect of irreversible resistance as a result of the residual strain present after repeated loading cycles [18].

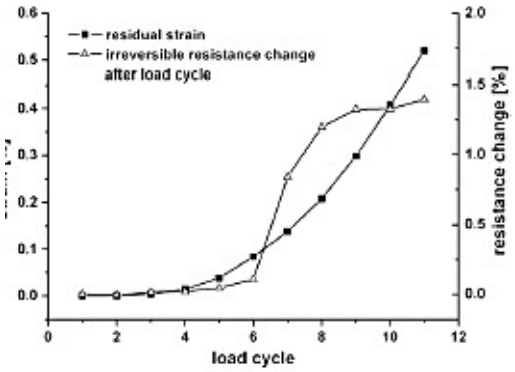

Fig. 41 Residual strain after repeatedly applied load cycles corresponding to irreversible resistance change [18]

As seen from the graphs above the resistance increases with amount of load cycles applied, however this is to a magnitude of 0.05 % after the first 5 cycles corresponding to an irreversible resistance change of 0.02 %. Both these values increase to 0.52 % and 1.4 % respectively after the 11^{th} cycle. Epoxy modified with

carbon black nanoparticles exhibited the highest sensitivity of between 10 % - 20 % regarding irreversible resistance [18].
Fig. 42 indicates the percentage resistance change vs strain percentage during the 10th loading cycle of the multiwall carbon nanotubes in (a) and the carbon black nanoparticles in (b).

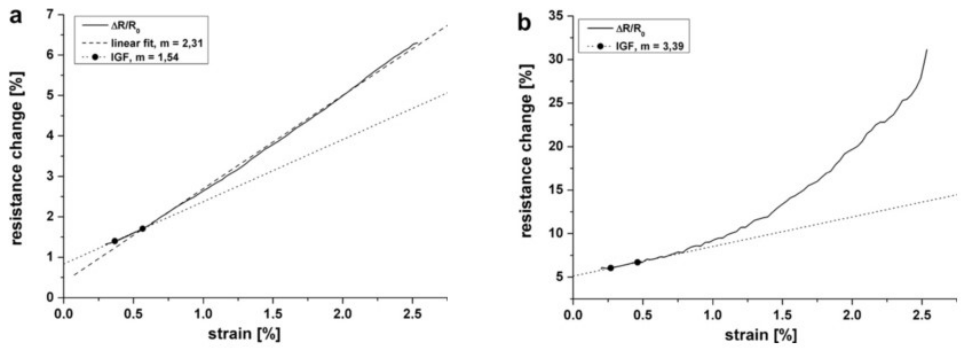

Fig. 42 Percentage resistance change vs strain percentage during the 10th loading cycle (a) MWCNT, (b) CBNP [18]

It is clear from the graphs below that the carbon black modified matrix is more sensitive the stress strain than the multiwall carbon nanotubes. This is due to the difference in structure since the carbon nanotubes are larger in size it is easier for these to make contact with neighboring nanotubes to conduct a current [18].
Dynamic tensile tests performed on the specimens indicated that an increase in electrical resistivity occurred upon delamination with resistance reaching up to 100 % when a large part of the material is delaminated. The change in resistance was thus concluded to be related to the crack density in the sample [18]. The effect of electrical conductivity and magnetic properties using Fe_3O_4 nanoparticels imbedded in an aluminum matrix was investigated by Ferreira, Bayraktar et al. [32] where Fe_3O_4 powder of 99.62 % purity was used and combined with aluminum powder. A ceramic oven was used to form the composite material at 600 ^oC. Three samples were produced with Fe_3O_2 nanoparticle compositions 10 %, 20 % and 30 % with the different properties investigated. Optical microscope images for the respective samples are presented in fig. 43 and SEM images in fig. 44 [32].

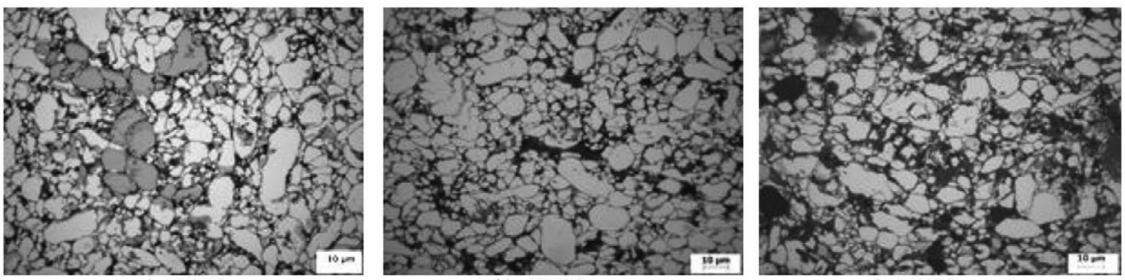

a) AF-10 b) AF-20 c) AF-30

Fig. 43 Optical microscope image of 10 % (a), 20 % (b) and 30 % (c) nanoparticle content samples respectively [32]

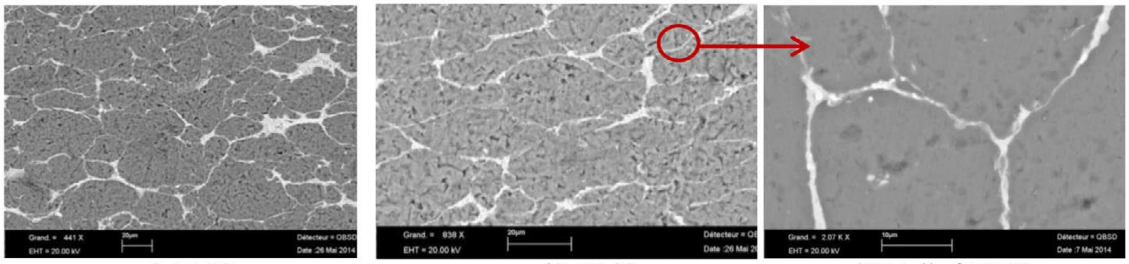

a) AF-10 b) AF-20 c) Detail of AF-20

Fig. 44 SEM images of 10 % (a), 20 % (b) and enhanced image of 20 % (c) nanoparticle content samples [32]

It was noted from the SEM and optical microscope images that the nanoparticles were dispersed homogeneously around the grain boundaries of the aluminum, this could have been attributed to rapid mixing as the composite was heating. Density of the Fe_3O_4 nanoparticles in the composite varied slightly between 2,5 g cm^3 and 3,0 g cm^3 as seen in fig. 45 [32].

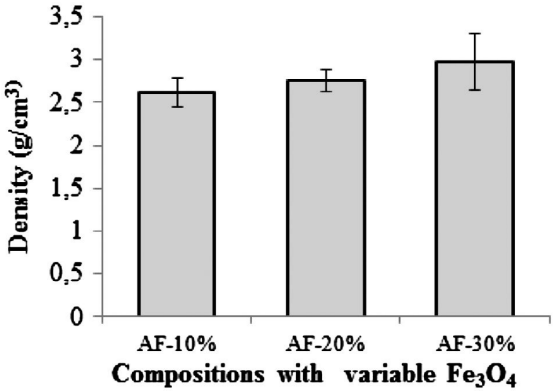

Fig. 45 Density variation with different loading of nanoparticle samples [32]

Electrical conductivity measurements are presented in table 9 and indicates that with an increase in Fe_3O_4 nanoparticle loading resulted in an increase in electrical resistivity and decrease in electrical conductivity [32].

Table 9. Electrical conductivity and resistivity results for aluminum/Fe_3O_4 composite [32]

Composition	Resistivity (ohm.m)	Conductivity (S/m)
Pure aluminium	0.000188	11,895
AF-10	0.000281	3999
AF-20	0.001028	1042
AF-30	0.001036	1045

Magnetic properties of the formed composite were investigated, and results presented in fig. 46.

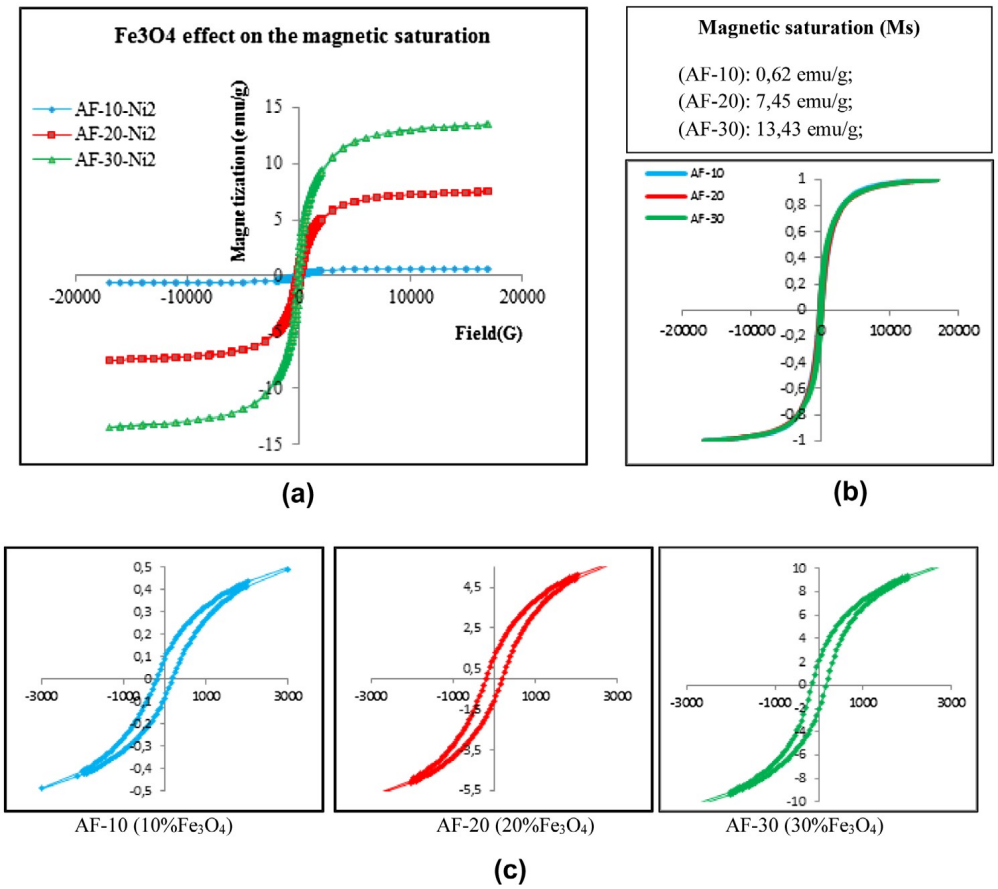

Fig. 46 Change in magnetic properties of aluminum/Fe_3O_4 composite [32]

As seen in figure 46 above for graph (a) the field dependence of magnetization increases with larger volume fraction of magnetic nanoparticles. (b) indicated that magnetic saturation and normalised curve is also of greater magnitude for higher volume fractions as was the case for magnetic field dependence in (a). (c) Indicates the hysteresis curves for the respective samples as an increase in magnitude is also noticed with increased nanoparticle volume fraction. Tab. 10 represents the relationship between these values [32].

Table 10. Relationship between magnetization (M_s), remanence magnetization (M_r), coercive field (H_c), the relationship between M_r/M_s with the susceptibility X_m [32]

Sample	M_s (emu/g)	M_r (emu/g)	H_c (G)	M_r/M_s	X_m
AF-10	0.55±0.02	0.0880±0.0003	199.446±50.03	0.160±0.023	7.21E−4
AF-20	7.46±0.05	1.0695±0.001	199.422±50.09	0.1433±0.051	7.73E−4
AF-30	13.43±1.01	2.108±0.07	149.42±50.82	0.1569±0.090	1.05E−3

2.5 Reduction of Nitric Oxide Gas Particles whilst Increasing Engine Performance with Nanoparticles

Carbon nanotubes were synthesized in a DC thermal arc plasma process under a helium atmosphere at 600 Torr pressure. Two high purity graphite rods were used on a block of graphite with arcing across the two rods. This was performed at a voltage

of 20 V and a current of 80 – 100 A. Due to some condensing of the evaporated carbon a hard deposit of slack formed on the tip of the cathode. The deposit formed consisted of carbon nanotubes and a small amount of amorphous carbon. A SEM image of the carbon nanotubes with arc discharge is presented in fig. 47 [27].

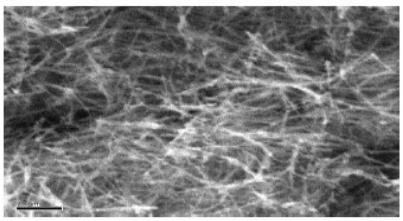

Fig. 47 SEM formation of MWCNT particles with arc discharge [27]

Successful carbon nanotube formation was confirmed with the SEM images illustrated in fig. 48.

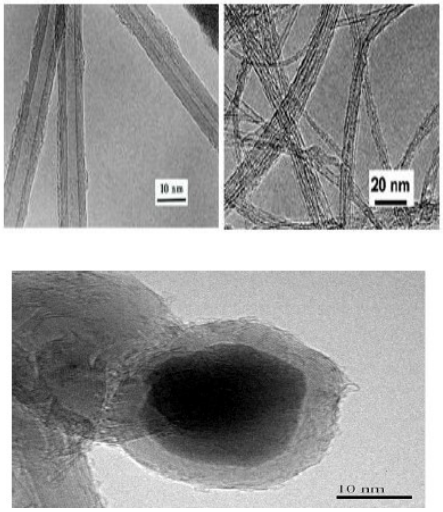

Fig. 48 SEM images of formed MWCNT particles [27]

HOME (modified biodiesel) + 50 % MWCNT showed lower nitric oxide emissions compared to other blends and significant improvement over pure diesel as seen from the results in fig. 49.

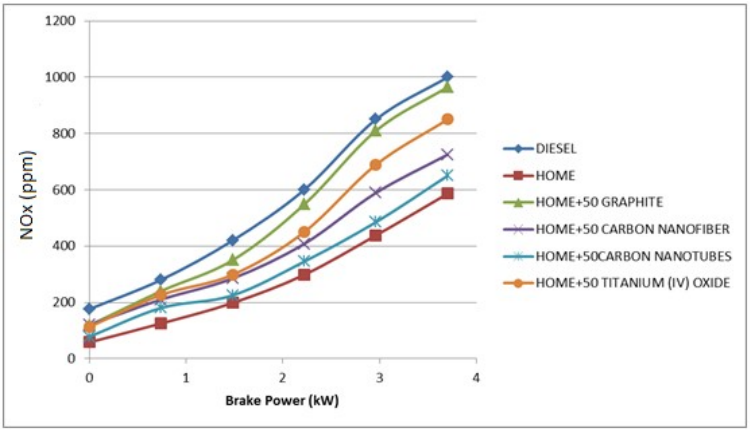

Fig. 49 Results of reduction in nitric oxide (NOx) with the use of nanomaterial in diesel [27]

This result was only slightly surpassed by biodiesel. This was attributed to the possibility of lower heat release rates of HOME during premixed combustion phase, which resulted in lower peak temperatures. Complete combustion may have led to increased temperatures inside the combustion chamber resulting in higher nitric oxide formation. This was attributed to complete combustion and higher premixed combustion heat release rates which was observed with HOME + 50 % Graphite blends. Further study showed that due to the high thermal conductivity and catalytic activity of MWCNT this resulted in improved combustion (higher CO_2 value) resulting in better engine performance as illustrated in fig. 50 [27].

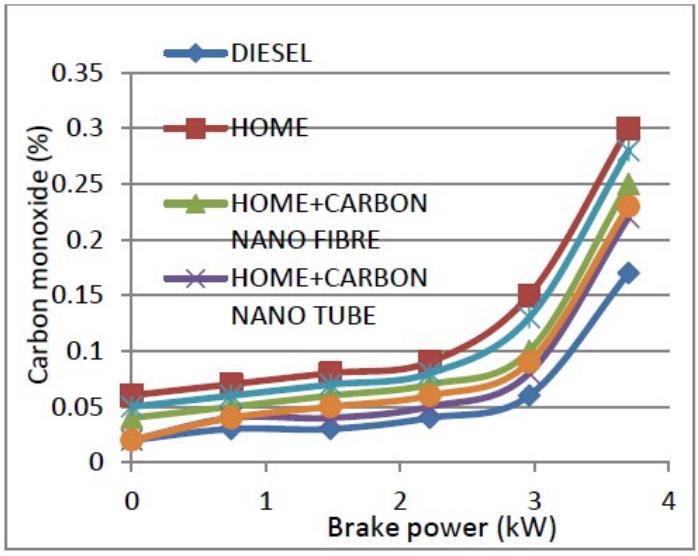

Fig. 50 Effect of nanoparticles in biodiesel (HOME) on engine performance [27]

2.6 Friction Stir Processing (FSP)

Mishra et al. [26] used SiC nanoparticles in powder form and mixed into a small amount of methanol. The suspension was then applied to the surface of the plates to form a thin SiC particle layer. The aluminum plates with the applied SiC particle layer was dried in air and was subjected to FSP. A tacking tool with a pin height of 1.0 mm was used. A constant tool rotating rate of 300 rpm was used while the traverse rate and depth of shoulder was varied. The tool spindle angle was 2.58. This assisted in a forging action at the trailing edge of the shoulder. The target depth was defined as the depth to which the pin would have inserted into the work piece. The position of the shoulder was controlled by the target depth in respect to the top layer of the worksheet. Transverse sections of processed aluminum plates were mounted and mechanically polished. These were then examined using an optical microscope. Sicon Image Software was used to determine the SiC volume fraction on the finished aluminum plates and the microhardness of the finished material was measured using a load of 400 g [26]. A target depth of 2.03 mm incorporated the SiC particles into the aluminum matrix. A transverse speed of 25 mm min^{-1} was used with the stated target depth to produce the desired effect since at higher transverse speeds the composite

layer would separate from the aluminum matrix [26]. An optical micrograph of the finished product is illustrated in fig. 51.

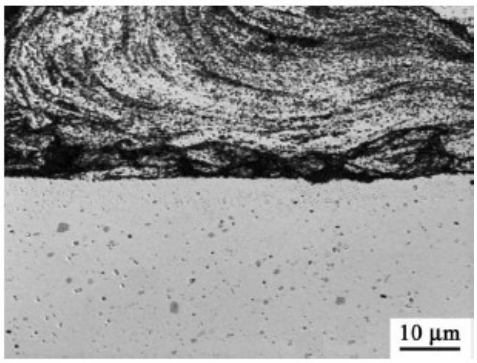

Fig. 51 Optical micrograph of composite and aluminum matrix interface [26]

From the optical micrograph in figure 52 the SiC nanoparticles are evenly distributed in the aluminum matrix with no irregularities detected.

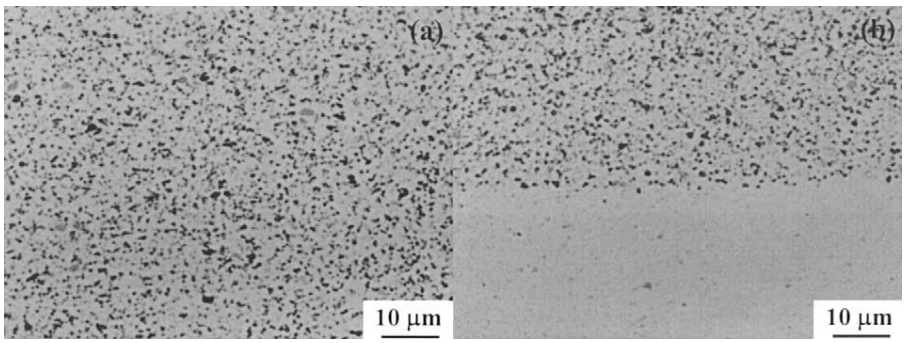

Fig. 52 Enhanced optical micrograph of the particle density and dispersion (a) and the bonding interface between the SiC composite and aluminum matrix [26]

The thickness of the composite layer on the aluminum sheet ranged from 50 to 200 mm. The volume fraction of SiC particles was estimated to be 13 % by software analysis. Fig. 52 (b) indicates the zone where the composite bonds the aluminum and illustrates perfect bonding of the composite to the surface of the aluminum with no defects. Similar results were obtained when the volume fraction was increased to 27 % with perfect bonding and particle dispersion, however it can be seen in table 11 that the hardness of the material was almost doubled [26].

Table 11. Effect of nanoparticle volume fraction on metal hardness [26]

Location	Vol.% of SiC particles	Hardness (HV)
Base plate	0	85
Surface composite	13±2	123
	27±3	173

This same method was used by Tonelli et al. [25] with small modifications and using an extruded $AlSi_{12}CuNiMg$ matrix with micro and nano-sized Al_2O_3 particles for reinforcement.

3. CONCLUSION

A major influence in changing the properties of the matrix to which nanoparticles are applied to form a composite is the size of the particle used. Small nanoparticles can have high reactivity due to a high surface area to volume ratio, whereas larger particles may act more as reinforcement [3]. The ability of nanoparticles in a matrix to make contact with neighboring nanoparticles will create pathways through which thermal radiation and electricity could be conducted depending on the thermal and electrical conductivity of the particles used. Authors Ho and Gao, [30] found that an increase in temperature as the viscosity of a solution decreases the thermal conductivity will increase correspondingly. Larger particles or heavier loading of nanoparticles would enhance this property; however, flakes of a conductive nanomaterial can be added to the polymer matrix to further increase the electrical or thermal conductivity [33]. The use of nanoflakes could occupy a larger volume fraction at lower weight, but conductive filler contact must be made, thus a combination of flakes and nanoparticles could be more beneficial. Silver nanowires are found to poses some of the best thermal and electrically conductive properties of nanomaterials used in industry with a proven percolation at less than 1% volume fraction [34]. Reason for this is increased contact between the filling particles allowing for better conductive pathways. AgNPs are also relatively easy to synthesize to high purity with increasing cost effectiveness. Hydrogels are typically used for their ability to provide controlled drug release however, with simple modification of the same matrix the size and phase changes observed when stimuli are applied could be of practical use in industry.

SiO_2 nanoparticles were considered to be non-conductive and associated with low microwave absorption, however with surface modification of nitrogen, carbon and chlorine atoms these prove to be good conductors with excellent microwave absorptive properties. When applying a nanoparticle polymer solution onto a substrate the spraying method proves to be more effective whilst higher annealing temperatures not only improves binding of the applied nanoparticle polymer, but also increases the electrical conductivity substantially [17]. The use of Nickel fibers in a polyether sulfone matrix exhibited the highest electromagnetic shielding effectiveness, however reducing the size to nanostructures to increase the volume fraction could potentially increase the shielding effectiveness further [16]. Recyclability of waste carbon fiber and nanocomposites could prove to be very useful in saving energy and further utilization of other polymers as reinforcing material. Friction Stir Processing proves to be excellent for incorporating nanocomposites onto metal matrices to improve the base material hardness by up to double that of the unmodified base material. The use of multiwall carbon nanoparticles could reduce nitric oxide gas emissions significantly whilst increasing engine performance. For conductivity enhancement of a matrix the first choice tends to be the use of metallic nanoparticles, however these tend to be much heavier than carbon alternatives [17]. Improvements have been made in this regard by using carbon nanostructures and nanoparticles to achieve similar electrical and thermal conductivity to metallic nanoparticles such as copper [27]. During friction stir processing it is important to find an ideal transverse speed and pin

depth to ensure perfect bonding and dispersion of the nanoparticle composite onto a metal surface whilst increases in nanoparticle volume fraction could improve the harness of the metal to which it is applied significantly [26].

ACKNOWLEDGEMENT

This work was supported by the Ministry of Education, Youth and Sports of the Czech Republic and the European Union - European Structural and Investment Funds in the frames of Operational Programme Research, Development and Education - project Hybrid Materials for Hierarchical Structures (HyHi, Reg. No. CZ.02.1.01/0.0/0.0/16_019/0000843) and project "Sophisticated hybrid tapes for fabrication of composites by precise winding" (project identification no. TJ01000292) / Technology Agency of the Czech Republic (Programme Zeta).

REFERENCES

[1] Hanemann T. and Szabó D.: *Polymer-Nanoparticle Composites: From Synthesis to Modern Applications*. Materials, **3**(6), 3468-3517 (2010)

[2] Goyal R., Sharma M. and Amberiya U.: *Innovative Nano Composite Materials and Applications in Automobiles*. International Journal of Engineering Research & Technology (IJERT), **3**(1), 3002 (2014)

[3] Camargo P., Satyanarayana K. and Wypych F.: *Nanocomposites: synthesis, structure, properties and new application opportunities*, *Materials Research*, **12**(1), 1-2. (2009)

[4] Thoniyot P., Tan M., Karim A., Young D. and Loh X.: *Nanoparticle-Hydrogel Composites: Concept, Design, and Applications of These Promising, Multi-Functional Materials*, Advanced Science, **2**(1-2), p.1400010. (2015)

[5] Salaün F., Devaux E., Bourbigot S., Rumeau P., Chapuis P., Saha S. and Volz S.: *Polymer nanoparticles to decrease thermal conductivity of phase change materials*. Thermochimica Acta, **477**(1-2), 25-31 (2008)

[6] Khodadadi J. and Hosseinizadeh S.: *Nanoparticle-enhanced phase change materials (NEPCM) with great potential for improved thermal energy storage*. International Communications in Heat and Mass Transfer, **34**(5), 534-543 (2007).

[7] Motahar S., Nikkam N., Alemrajabi A., Khodabandeh R., Toprak M. and Muhammed M.: *A novel phase change material containing mesoporous silica nanoparticles for thermal storage: A study on thermal conductivity and viscosity*, International Communications in Heat and Mass Transfer, **56**, 114-120 (2014)

[8] Qian T., Li J., Min X., Guan W., Deng Y. and Ning L.: *Enhanced thermal conductivity of PEG/diatomite shape-stabilized phase change materials with Ag nanoparticles for thermal energy storage*, Journal of Materials Chemistry **A3**(16), 8526-8536 (2015).

[9] Tonapi S., Zhong H., Simone D. and Fillion R.: *THERMAL CONDUCTIVE MATERIAL UTILIZING ELECTRICALLY CONDUCTIVE NANO PARTICLES.* USP 7,550,097 B2. (2009)

[10] Prabhu S. and Poulose E.: *Silver nanoparticles: mechanism of antimicrobial action, synthesis, medical applications, and toxicity effects*, International Nano Letters, **2**(1), 1-10 (2012)

[11] Xue C., Chen J., Yin W., Jia S. and Ma J.: *Superhydrophobic conductive textiles with antibacterial property by coating fibers with silver nanoparticles*, Applied Surface Science, **258**(7), 2468-2472 (2012)

[12] Park M., Im J., Shin M., Min Y., Park J., Cho H., Park S., Shim M., Jeon S., Chung D., Bae J., Park, J. Jeong U. and Kim K.: *Highly stretchable electric circuits from a composite material of silver nanoparticles and elastomeric fibres,* Nature Nanotechnology, **7**(12), 803-809 (2012)

[13] Li J., Liu W., Zhao L. and Zhou M.: *High-performance nanostructured thermoelectric materials*, NPG Asia Materials, **2**(4), 152-158 (2010)

[14] Khosla A.: *Nanoparticle-doped Electrically-conducting Polymers for Flexible Nano-Micro Systems*, Interface magazine, **21**(3-4), 67-70 (2012)

[15] Green M., Liu Z., Xiang P., Liu Y., Zhou M., Tan X., Huang F., Liu L. and Chen X. *Doped, conductive SiO_2 nanoparticles for large microwave absorption*, Light: Science & Applications, **7**(1), 1-9 (2018)

[16] Los P., Lukomska A. and Jeziorska R.: *Metal-polymer composites for electromagnetic interference shielding applications*, Polimery, **61**(10), 663-669. (2016)

[17] Dermanaki F. R., Gagne M., Klemberg-Sapieha J. and Therriault D.: *Electrically Conductive Silver Nanoparticles-Filled Nanocomposite Materials as Surface Coatings of Composite Structures,*. Advanced Engineering Materials, **18**(7), 1189-1199 (2016)

[18] Böger L., Wichmann M., Meyer L. and Schulte K.: *Load and health monitoring in glass fibre reinforced composites with an electrically conductive nanocomposite epoxy matrix*, Composites Science and Technology, **68**(7-8), 1886-1894 (2008)

[19] Njuguna J., Silva F. and Sachse S.: *Nanocomposites for Vehicle Structural Applications*. Chap 19 in book *Nanofibers – Production, Properties and Functional Applications*, 419-434, INTECH Open Access Publisher. (2011).

[20] Abhange A. : *Nanotechnology – Emergence in Automotive Industry*, Symbiosis Institute of Technology, Symbiosis International University, Lavale, Pune 12/11, 2018

[21] Garcés J., Moll D., Bicerano J., Fibiger R. and McLeod D.: *Polymeric Nanocomposites for Automotive Applications*, Advanced Materials, **12**(23), 1835-1839 (2000)

[22] Naskar A., Keum J. and Boeman R.: *Polymer matrix nanocomposites for automotive structural components*, Nature Nanotechnology, **11**(12), 1026-1030 (2016)

[23] Patel V. and Mahajan Y.: Polymer nanocomposites drive opportunities in the automotive sector. Nanowerk. Available at: https://www.nanowerk.com/spotlight/spotid=23934.php (2012)

[24] Wang Q. and Chung Y.: Encyclopedia of tribology p. 376. New York: Springer 2013.

[25] Tonelli L. et al.: *Production of $AlSi_2CuNiMg/Al_2O_3$ Micro/Nanodispersed Surface Composites Using Friction Stir Processing for Automotive Applications*. In: Hovanski Y., Mishra R., Sato Y., Upadhyay P., Yan D. (eds) *Friction Stir Welding and Processing X*. The Minerals, Metals & Materials Series. Springer, Cham 2019

[26] Mishra R., Ma Z. and Charit I.: *Friction stir processing: a novel technique for fabrication of surface composite*, Materials Science and Engineering: **A341**(1-2), 307-310 (2003)

[27] Roy A., Sreejith C., Abhishek S., Ragul G. and Indira G.: *Effect of Multi-Walled Carbon Nanotubes on Automotive and Aerospace Applications- Case Study*. International Journal of Emerging Trends in Science and Technology, **05**(04), 5102-5113 (2017)

[28] Huang Y., Kormakov S., He X., Gao X., Zheng X., Liu Y., Sun, J. and Wu D.: *Conductive Polymer Composites from Renewable Resources: An Overview of Preparation, Properties, and Applications*, Polymers, **11**(2), 187-219 (2019)

[29] Velickovic S., et al.: *Application of Nanocomposites in the Automotive Industry*. International Congress Motor Vehicles & Motors 2018, Kragujevac, Serbia, October 4th - 5th, 2018

[30] Ho C. and Gao J. *Preparation and thermophysical properties of nanoparticle-in-paraffin emulsion as phase change material*, International Communications in Heat and Mass Transfer, **36**(5), 467-470 (2009)

[31] Kang H., Kim S. and Oh J.: *Estimation of Thermal Conductivity of Nanofluid Using Experimental Effective Particle Volume*, Experimental Heat Transfer, **19**(3), 181-191 (2006)

[32] Ferreira L., Bayraktar E. and Robert M.: *Magnetic and electrical properties of aluminium matrix composite reinforced with magnetic nano iron oxide (Fe_3O_4)*, Advances in Materials and Processing Technologies, **2**(1), 165-173 (2016)

[33] Zhang R., Moon K., Lin W. and Wong C.: *Preparation of highly conductive polymer nanocomposites by low temperature sintering of silver nanoparticles*, Journal of Materials Chemistry, **20**(10), 2018 (2010)

[34] Lonjon A., Demont P., Dantras E. and Lacabanne C.: *Low filled conductive P(VDF-TrFE) composites: Influence of silver particles aspect ratio on percolation threshold from spheres to nanowires*,Journal of Non-Crystalline Solids, **358**(23), 3074-3078 (2012)